

**UNCLASSIFIED**  
**AD** **417620**

**DEFENSE DOCUMENTATION CENTER**  
**FOR**  
**SCIENTIFIC AND TECHNICAL INFORMATION**  
**CAMERON STATION, ALEXANDRIA, VIRGINIA**

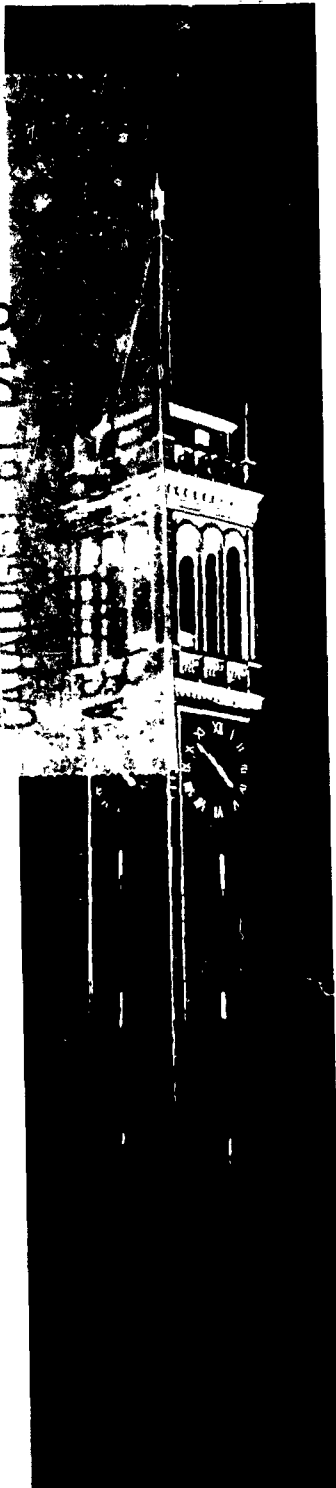


**UNCLASSIFIED**

NOTICE: When government or other drawings, specifications or other data are used for any purpose other than in connection with a definitely related government procurement operation, the U. S. Government thereby incurs no responsibility, nor any obligation whatsoever; and the fact that the Government may have formulated, furnished, or in any way supplied the said drawings, specifications, or other data is not to be regarded by implication or otherwise as in any manner licensing the holder or any other person or corporation, or conveying any rights or permission to manufacture, use or sell any patented invention that may in any way be related thereto.

64-2

CATALOGED BY DDDO



# **Anode Structures For Cold-Cathode High-Power Magnetron**

by  
**Y. Ikeda**

**417620**

Series No. 60, Issue No. 455  
Contract No. AF 19(628)-324  
June 30, 1962

DDC  
SEP 26 1963  
RECEIVED  
TISA 2

**ELECTRONICS RESEARCH LABORATORY**  
UNIVERSITY OF CALIFORNIA  
BERKELEY, CALIFORNIA

**"Requesters for additional copies by Agencies of the Department of Defense, their contractors, and other Government agencies should be directed to the:**

**ARMED SERVICES TECHNICAL INFORMATION AGENCY  
ARLINGTON HALL STATION  
ARLINGTON 12, VIRGINIA**

**Department of Defense contractors must be established for ASTIA services or have their 'need-to-know' certified by the cognizant military agency of their project or contract."**

**"All other persons and organizations should apply to the:**

**U.S. DEPARTMENT OF COMMERCE  
OFFICE OF TECHNICAL SERVICES  
WASHINGTON 25, D.C."**

AFCRL-63-320

Electronics Research Laboratory  
University of California  
Berkeley, California

ANODE STRUCTURES FOR COLD-CATHODE  
HIGH-POWER MAGNETRON

by

Y. Ikeda

Institute of Engineering Research  
Series No. 60, Issue No. 455

Contract No. AF 19(628)-324  
Project No. 5634  
Task No. 563402

Scientific Report No. 20

June 30, 1962

Prepared for  
Air Force Cambridge Research Laboratories  
Office of Aerospace Research  
United States Air Force  
Bedford, Massachusetts

### Acknowledgment

The author is indebted to the Electronics Research Laboratory, University of California at Berkeley, for providing him with the opportunity of performing the investigation. The research has been carried out under the guidance of Prof. D. H. Sloan, from whom the original idea regarding the new structure came. The author also gratefully acknowledges the suggestions made by Prof. A. W. Trivelpiece and Prof. C. Susskind with regard to the final manuscript, as well as the technical assistance by Messrs. O. B. Westwick and J. Tombaugh.

## SUMMARY

Rf interaction properties of several structures suitable for cold-cathode high-power magnetrons have been investigated analytically and experimentally, with special emphasis on increasing the understanding of the interaction and maximizing the area of coherent interaction with the electron beam at a given frequency. The structures analyzed were designed for large mode separation, maximum interaction impedance, and easy coupling to the output circuit.

## TABLE OF CONTENTS

	<u>Page</u>
I. INTRODUCTION . . . . .	1
II. INVERTED MAGNETRON STRUCTURE . . . . .	1
A. Proposed Anode Structure, Symbols and Definitions. . .	1
B. Resonance Frequency for the Individual Cavity. . . . .	3
C. Measurement of the Resonant Frequency. . . . .	4
D. An Equivalent Circuit Representation . . . . .	10
E. Cavity Losses and Q. . . . .	15
F. Mode-Separation Improvement. . . . .	18
III. CONVENTIONAL-MAGNETRON ANODE STRUCTURE . . . . .	20
A. Anode Structure, Symbols, and Definitions. . . . .	20
B. Resonant Frequency of an Individual Cavity . . . . .	20
C. Measurement of Resonant Frequencies. . . . .	24
D. Equivalent Circuits for Linear Magnetron Structure . .	25
1. Analysis for $n = 0$ Mode . . . . .	25
2. Analysis for $n = 1$ Mode . . . . .	28
3. Numerical Results and Experiment . . . . .	29
E. Cavity Losses and Q. . . . .	30
F. Improvement of Mode Separation . . . . .	34
G. Comparison of Structures of Secs. II and III . . . . .	34
IV. ANODE-STRUCTURE CONSIDERATIONS . . . . .	37
A. Reduction of Outer Radius . . . . .	37
B. Magnetron Structure with Large Mode Separation . . . .	38
C. Outer-Cathode Anode Structure with Short-Circulating Bars Along Outer Edge. . . . .	40
D. Cylindrical Cavity . . . . .	41
V. CONCLUSIONS. . . . .	43
REFERENCES . . . . .	43



# LIST OF ILLUSTRATIONS

<u>Figure</u>		<u>Page</u>
1	Inverted Magnetron Structure . . . . .	2
2	Equivalent Capacitance . . . . .	3
3	Graphical Determination of Resonant Frequency. . . . .	5
4	Results of the Calculation of Resonant Frequencies . . . . .	6
5	Cavity Used in Experimental Confirmation of Calculated Frequencies . . . . .	7
6	Alternate Inverted Structure . . . . .	8
7	Measured Spectra and Calculated Frequencies for Unit Cavity and for Cavities at Both Ends . . . . .	9
8	Equivalent Circuit for the Structure of Fig. 1 . . . . .	11
9	Four-Terminal Network Elements of the Line of Fig. 8 . . . . .	12
10	Phase Characteristics and Characteristic Impedance for the Structure of Fig. 6. . . . .	13
11	Equivalent-Circuit Representation for Various Resonant Conditions: (a) Parallel Resonance, (b) Series Reso- nance, (c) Combined Resonance. . . . .	14
12	Schematic Representation of Gap. . . . .	17
13	Distribution of Loss Density . . . . .	17
14	Gap Modified for Improved Mode Separation. . . . .	18
15	Calculation of Resonant Frequency from Eq. (14). . . . .	19
16	Structure for Cylindrical Magnetron . . . . .	21
17	Structure for Linear Magnetron . . . . .	21
18	Solutions of Eq. (18) for $\kappa = 0$ . . . . .	22
19	Comparison with the Results of Sec. II . . . . .	23
20	Test Configuration . . . . .	24
21	Equivalent Circuit for $n = 0$ Mode . . . . .	28
22	Equivalent Circuit for the $n = 1$ Mode. . . . .	29
23	Experimental Configuration . . . . .	30
24	Summary of Experimental Results . . . . .	31
25	Schematic Representation of Gap . . . . .	32
26	Loss-Density Distribution over Plate Surface . . . . .	33
27	Structure Used for Mode-Separation Improvement . . . . .	34

# LIST OF ILLUSTRATIONS (Cont.)

<u>Figure</u>		<u>Page</u>
28	Mode Separation and R/r Ratio at 1000 Mc as a Function of $R_0$ . . . . .	35
29	Mode Separation and R/r ratio as a Function of Mean Radius $(R_r)^{1/2}$ . . . . .	36
30	Proposed Reduced-Size Anode . . . . .	37
31	Structure with Improved Mode Separation: (a) Proposed Model, (b) Simplified Model . . . . .	39
32	Anode Structure with Outer Short-Circuiting Bars . . . .	40
33	TE-Mode Structure . . . . .	42
34	End Cavities for TE-Mode Structure . . . . .	42

# LIST OF TABLES

<u>Table</u>		<u>Page</u>
1	Resonant Frequencies for the Structure of Fig. 5 . . . . .	7
2	Resonant Frequencies for Another Structure . . . . .	9
3	Resonant Frequencies for the Structure of Fig. 20. . . . .	24
4	Resonant Frequencies Measured with Structures with Bars. . . . .	26
5	Calculated and Measured Frequencies . . . . .	32
6	$x = 2\pi r/\lambda_0$ for Various $\xi$ and $\eta$ . . . . .	37
7	$2\pi r/\lambda_0$ ( $=\beta r$ ) for $R/r = 2$ . . . . .	38
8	Resonant Frequencies in Terms of $\beta a$ . . . . .	39
9	Results for Fig. 32 . . . . .	41

## I. INTRODUCTION

This report deals with the rf interaction properties of several anode structures for high-power, cold-cathode magnetrons. Emphasis is on understanding the interaction and on determining how the region of coherent interaction with the electron beam can be made as large as possible at a given frequency so as to maximize the output power.

In a conventional magnetron, the number of resonators is limited by the requirement of reasonable separation in frequency of the modes. As the number of resonators increases, the mode separation of even the "strapped" and "rising-sun" configurations begin to be insufficient.

The structures investigated in this report were chosen as (1) suitable for construction in the cold-cathode magnetron experiments in this Laboratory, (2) possessing large mode separation, and (3) having a circuit that is easily coupled to the output circuit.

One circuit that was tried was a corrugated cylindrical wall with interaction bars and coupling channels. This circuit has a 60-percent mode separation but a rather low interaction impedance for the  $TM_0$  mode, since the minimum electric field occurs at the wall.

The new structures analyzed in this report are free from this difficulty; however, they do suffer from the disadvantage of being susceptible to possible multipactor action along the magnetic field resulting from the rf electric field. This problem probably can be avoided by a careful design of the circuit.

The main assumption made in the analysis is that the axial length of the structure is much shorter than a free-space wavelength, so that field variations along the structure can be neglected. Further, it is assumed that since many bars oriented parallel to the axis are to be used in structure, the capacity between them and the cylindrical wall is taken to be uniformly distributed along the cavity circumference. In many cases the capacity between anode and cathode is neglected.

MKS units are used throughout and only the symbols given other than common meaning are explained in the text.

## II. INVERTED MAGNETRON STRUCTURE

### A. PROPOSED ANODE STRUCTURE, SYMBOLS AND DEFINITIONS

In the first anode structure to be discussed (Fig. 1), the points at

## (II. INVERTED MAGNETRON STRUCTURE)

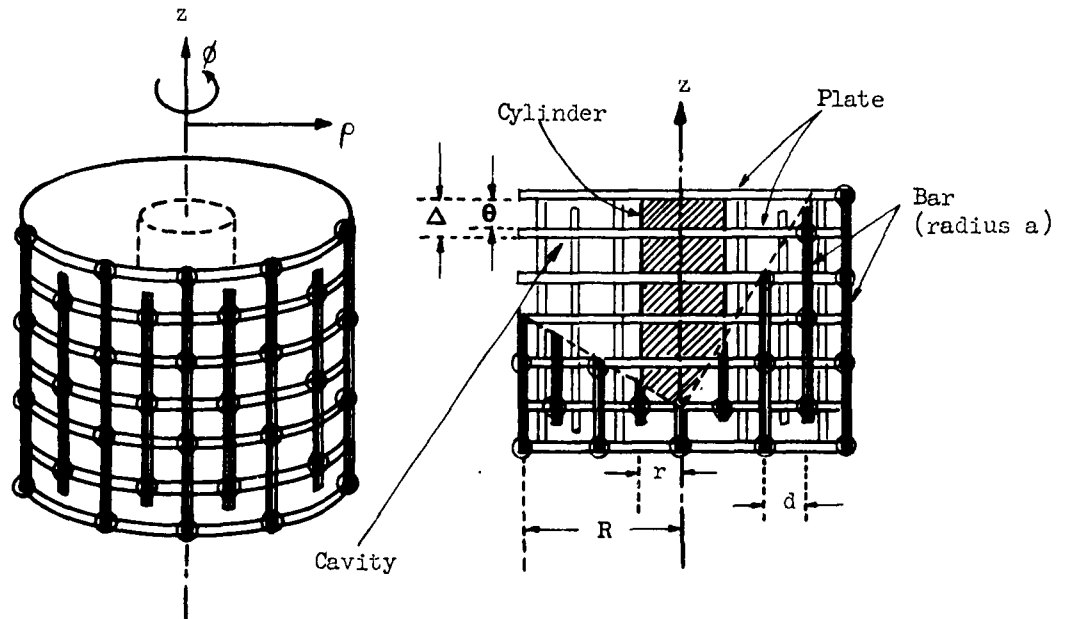


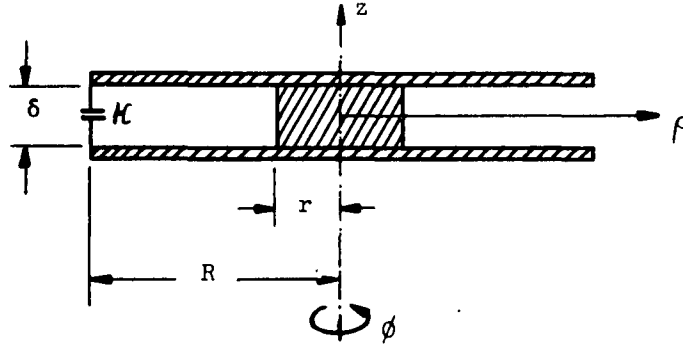
FIG. 1.--Inverted magnetron structure.

which the plate electrodes and bars are connected have been indicated by dots. The slow-wave structure is on the inside and is surrounded by a concentric cold cathode that depends on secondary emission for its electron current. The  $TM_0$  mode that is excited in each cavity makes the bars alternately plus and minus and consequently provides the circumferential rf fields necessary for magnetron operation. There is a dc magnetic field in the direction of the  $z$  axis.

The gap between the plates of the anode structure in Fig. 1 is denoted by  $\delta$ , a parameter chosen so as to minimize the multipactor problem and to optimize the interaction impedance. In general  $\delta$  is small and as a consequence the capacitance for a unit cavity is large, so that the frequency of the cavity is insensitive to the electron beam interaction as well as to the proximity of the cathode cylinder. For this reason no conventional "straps" are required for this structure.

## B. RESONANCE FREQUENCY FOR THE INDIVIDUAL CAVITY

The anode structure shown in Fig. 1 is made with a large number of bars. Their effect is therefore approximated by an equivalent uniform capacitance  $\mathcal{K}$  per unit length in the circumferential direction (Fig. 2). The edge effect

FIG. 2.--Equivalent capacitance  $\mathcal{K}$ .

of the plate may also be included in this equivalent capacity. It is assumed that only the  $z$  component of the electric field exists inside the cavity because the gap dimension  $\delta$  is small.

In cylindrical coordinates the solution of Maxwell's equations is given by the following:

$$E_z = E_0 [J_n(k\rho) + AN_n(k\rho)] \cos n\phi$$

$$H_\phi = -j \frac{kE_0}{\omega\mu_0} [J_n'(k\rho) + AN_n'(k\rho)] \cos n\phi \quad (1)$$

$$H = -j \frac{nE_0}{\omega\mu_0 \rho} [J_n(k\rho) + AN_n(k\rho)] \sin n\phi$$

where  $k^2 = \omega^2 \epsilon_0 \mu_0$ ,  $n = 0, \pm 1, \pm 2, \dots$  and  $A = -J_n(kr)/N_n(kr)$ . Also, since at  $\rho = R$ ,  $H_\phi(R)/V(R) = I_\rho(R)/V(R) = j\omega\mathcal{K}$ , where  $\mathcal{K}$  is the capacitance per unit length, we have

$$B_n(kR) = \frac{J_n'(kR) + AN_n'(kR)}{J_n(kR) + AN_n(kR)} = \mathcal{K} \delta \sqrt{\frac{\mu_0}{\epsilon_0}} \quad (2)$$

The resonant frequency for the various modes is determined by the above equations. It is convenient to rewrite these equations in terms of some new

## (II. INVERTED MAGNETRON STRUCTURE)

variables. Letting  $kR = 2\pi R/\lambda_0 = x$ , where  $\lambda_0$  is the free-space wavelength and  $r/R = \xi$ , we have

$$B_n(x, \xi) = \frac{J_n'(x)N_n(\xi x) - N_n'(x)J_n(\xi x)}{J_n(x)N_n(\xi x) - N_n(x)J_n(\xi x)} = \frac{\kappa \delta}{\epsilon_0 R} x \quad (2a)$$

The capacitance per unit length between parallel bars of radius  $a$  separated a distance  $d$  is

$$C_0 = \pi \epsilon_0 / \log [(d + \sqrt{(d^2 - 4a^2)})/2a] \quad (3)$$

From Fig. 1

$$\kappa = C_0 \Delta / d$$

As an example, we take  $R = 66$  mm,  $\xi = 1/8$ ,  $\delta = 3.5$  mm,  $\Delta = 5$  mm,  $d = 7.2$  mm, and  $a = 2.5$  mm. Then  $\kappa \delta / \epsilon_0 R \approx 0.15$ . The resonant frequency for the  $n = 0$  and  $n = 1$  modes can be determined as shown graphically in Fig. 3. The results of these calculations are given in Fig. 4. The rate of mode separation is also given.

If the central cylinder is removed,  $kR$  is the first root of  $J_0(kR) = 0$  for the  $TM_{001}$  mode; the rate of mode separation is about 60 per cent. The radial dimension of the cavity resulting from Fig. 4 is bigger than the cavity for  $J_0(kR) = 0$  if  $\xi > 0.45$  and the mode separation is good if  $\xi < 0.14$ .

This structure has a large mode separation for small values of  $\xi$ ; the rate of mode separation is not significantly affected by the capacitance of the bars.

### C. MEASUREMENT OF THE RESONANT FREQUENCY

A schematic diagram of the cavity used to check the calculated frequencies is shown in Fig. 5. The cavity was excited and the fields in the cavity were probed by small antennas inserted into holes as shown in the figure. The various modes of oscillation were detected by perturbing the fields with small wires that could be inserted into the drill holes at various places in the cavity.

The calculated and measured frequencies are compared in Table 1. The end capacitance per unit circumferential length is taken to be  $1/4$  of the

( II. INVERTED MAGNETRON STRUCTURE )

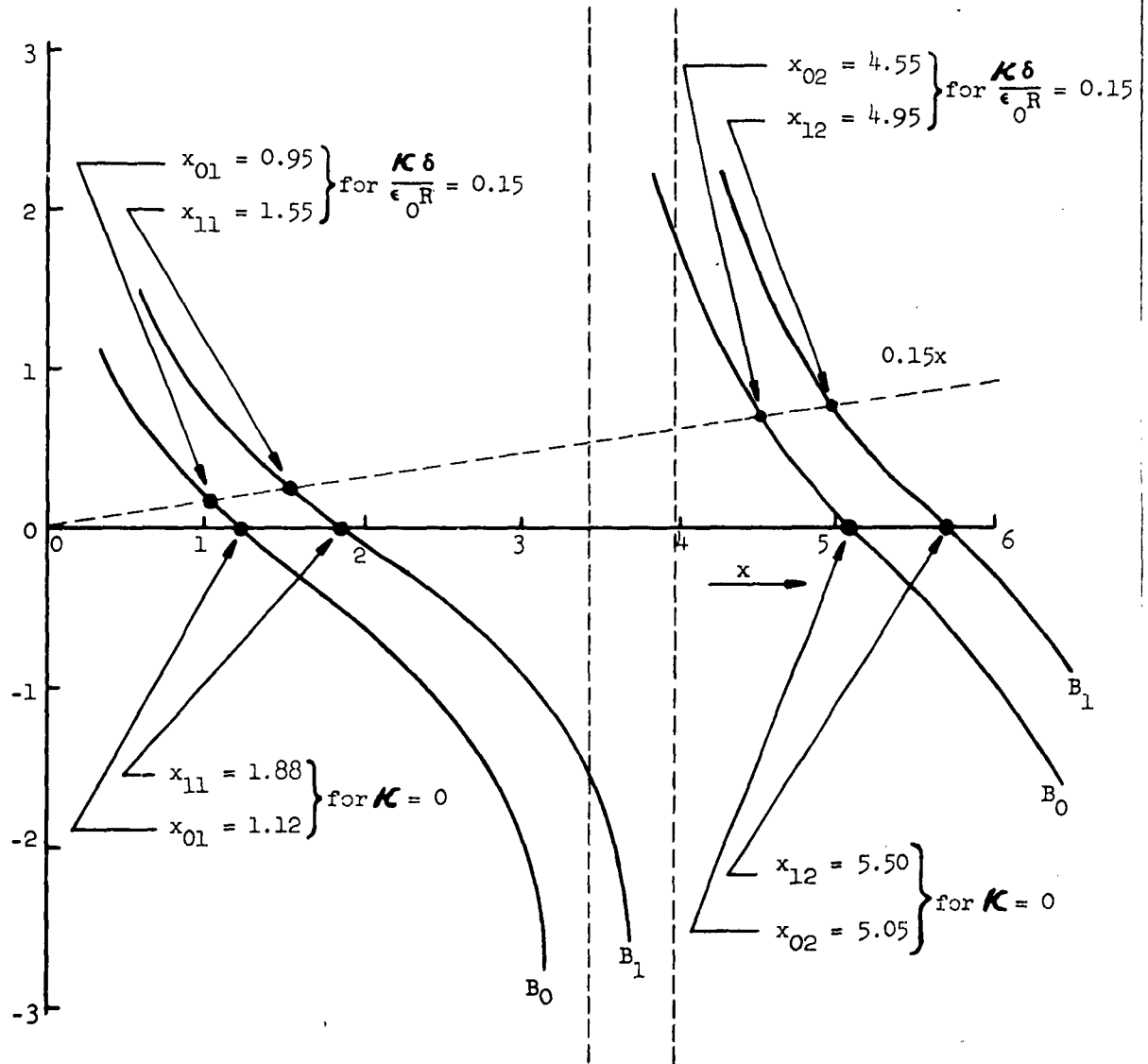


FIG. 3.--Graphical determination of resonant frequency.



(II. INVERTED MAGNETRON STRUCTURE)

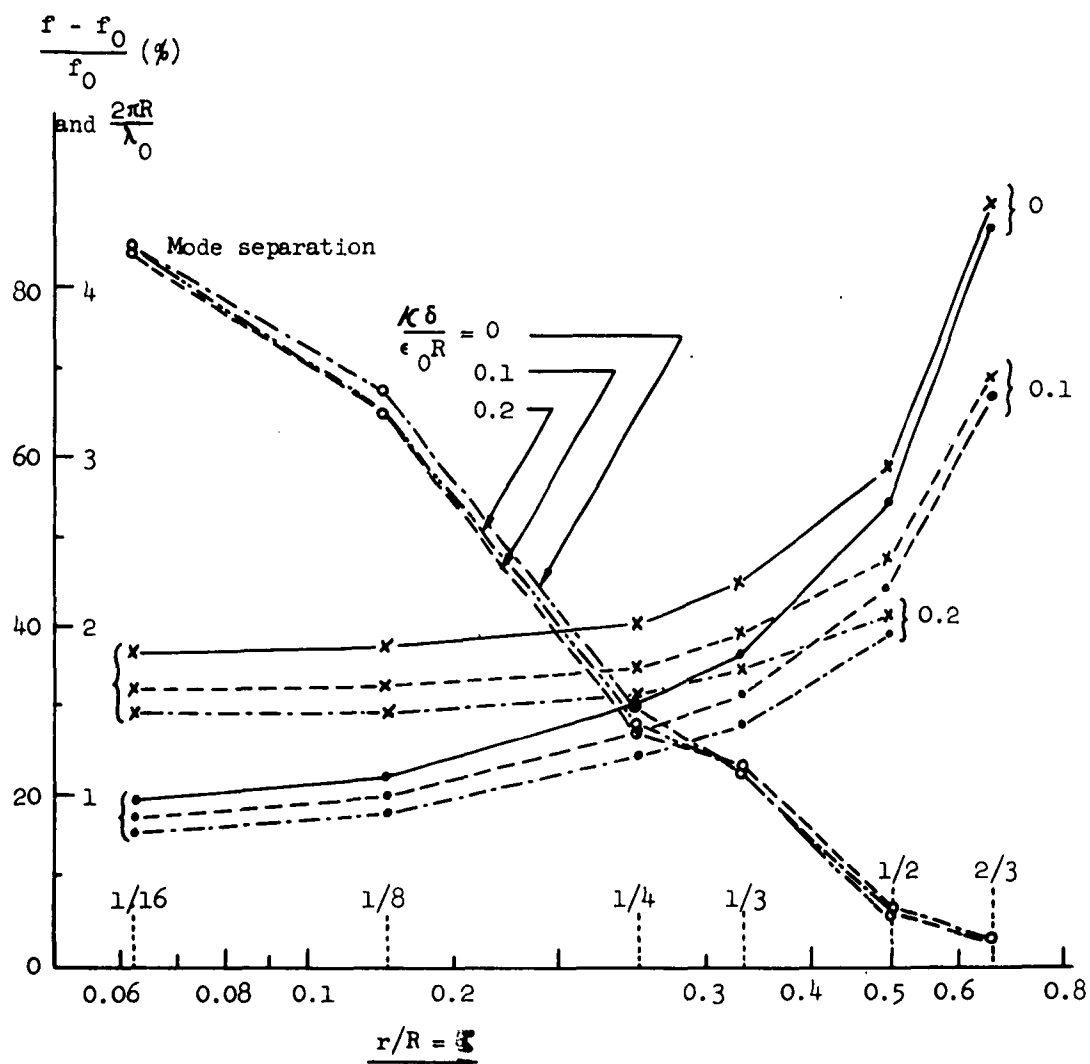


FIG. 4.--Results of the calculation of resonant frequencies.

(II. INVERTED MAGNETRON STRUCTURE )

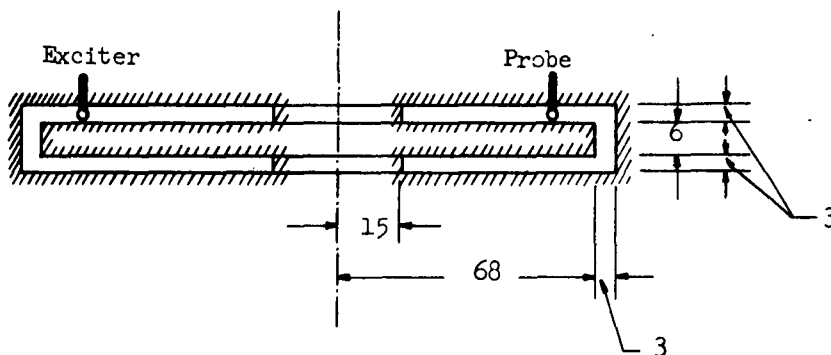


FIG. 5.--Cavity used in experimental confirmation of calculated frequencies.  $R = 68$  mm,  $\epsilon = 0.22$ . (Dimensions in millimeters.)

Table 1.--Resonant frequencies for the structure of Fig. 5  
( $K\delta/\epsilon_0 R \approx 1$ ).

Mode	Frequency (Mc)	
	Measured	Calculated
0	957	950
1	1326	1287
2	2010	-

capacitance of a coaxial line that has an inner radius of 3 mm and an outer radius of 6 mm. The calculated and measured values agree to within 3 per cent. In the calculation of the resonant frequency for this case it was possible to assume the effective radius  $R$  to be equal to  $1/2$  the distance along the gap in the cross section of Fig. 5; it is also assumed that  $K$  is equal to 0. In addition to the tabulated results a 1308-Mc mode was found. This is a weakly excited  $n = 1$  mode that exists in the coupled structure.

These measurements were repeated with the structure shown in Fig. 6. The results of these measurements are given in Fig. 7. This structure has many resonances because of the complicated coupling of the structure. These frequencies are shown in Fig. 7 in relation to the resonant frequency for the single cavity, and will be given more detailed consideration below. Results of another experiment with a similar structure but of different dimensions are shown in Table 2.

( II. INVERTED MAGNETRON STRUCTURE )

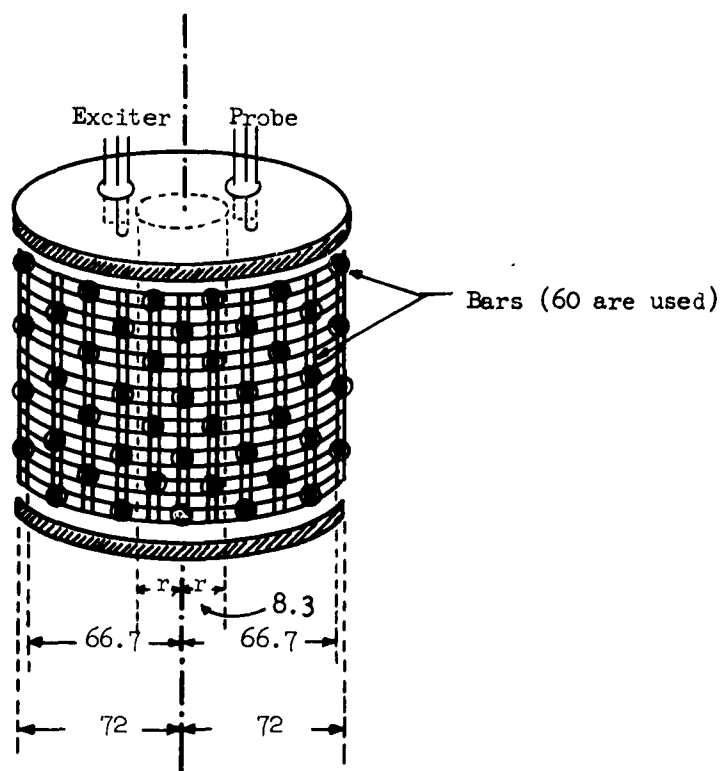


FIG. 6.--Alternate inverted structure. (All dimensions in millimeters.)  $\delta = 3.5$ ,  $\Delta = 5.0$ ,  $d = 7.2$ ,  $a$ ,  $2.5$ ,  $\delta/\epsilon_0 R = 0.15$ .

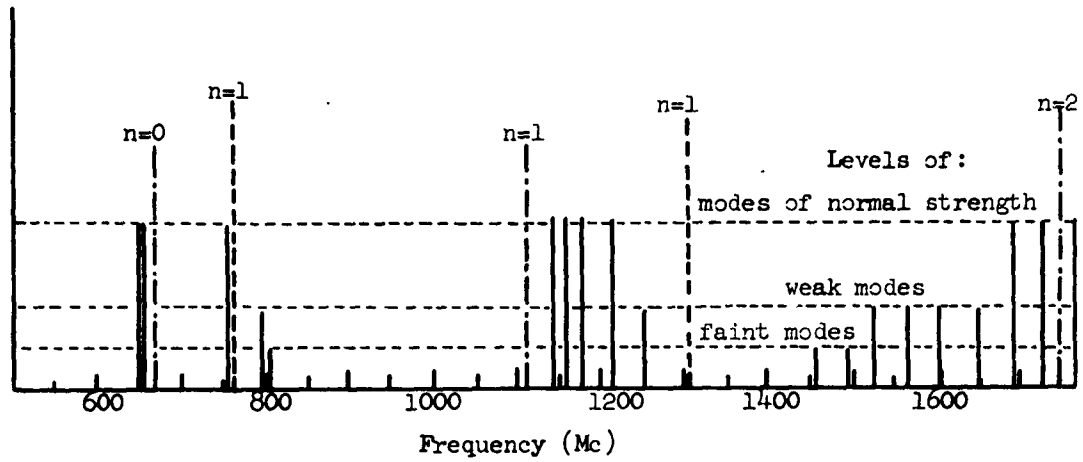


FIG. 7.--Measured spectra (solid lines) and calculated frequencies for unit cavity with  $R = 66.7$  mm (-----) and for cavities at both ends with  $R = 72$  m (-----).

Table 2.--Resonant frequencies for another structure:  $R = 60$ ,  $\xi = 0.125$ ,  $\delta = 3$ ,  $\Delta = 12$ ,  $d = 10$ ,  $a = 3$ ,  $K\delta/\epsilon_0 R \approx 0.2$ ; 40 bars. Measured frequencies marked by an asterisk are caused by end cavities (cf. Fig. 6).

Mode (measured circumferentially)	Frequency (Mc)	
	Measured	Calculated
0	660	716
(1)	750*	(890)
0	975*	(890)
1	1125	1175
0	1230	-
0	1270	-

## (II. INVERTED MAGNETRON STRUCTURE )

In Fig. 7 the detected frequencies are classified into three levels according to the amplitude of the oscillation. The amplitude depends on the method of excitation and thus the classification is not particularly valuable, although the probes were situated at the correct positions to measure TM modes. The agreement of theory and experiment is perhaps better than would be expected in view of the approximations used in determining the constants.

The end-cavities that were installed for the purpose of terminating the structure have a resonant frequency different from that of the main cavities. Therefore they are detected as a different group and are shown both in Fig. 7 and Table 2. These additional modes are characterized by a certain number of voltage nodes  $p$  of the voltage between adjacent bars in the  $z$  direction. In Fig. 7 the mode for 758 Mc has one node for the value of  $p$  and the configuration given in Table 2 has two nodes for the value of  $p$ . This is a result of the axial length of the latter structure being twice as long as that of the former.

These additional modes can be avoided by selection of an even number of main cavities. Then the end plates of the main cavities are connected with the same bars. It is also important for the number of main cavities to be even from the viewpoint of eliminating the additional end cavities, which generally have different resonant frequencies. In general an unsymmetrical structure at both ends introduces extraneous modes. Care must be taken to introduce the detecting probe and exciting antenna so as not to excite extraneous modes. For instance if the probe and antenna are inserted in the radial direction separated by an angle of  $120^\circ$ , the usual  $n = 1$  mode-region has several  $n = 3$  modes apparently excited. Similarly when the angle is  $90^\circ$  some of the  $n = 2$  modes are excited.

### D. AN EQUIVALENT CIRCUIT REPRESENTATION

We can synthesize an equivalent circuit for the structure of Fig. 1 if we assume that the two bars constitute a parallel-wire transmission line periodically loaded by the reactance of the cavities between the parallel plates. This equivalent circuit is shown in Fig. 8. The symbol  $L_{eq}$  denotes the reactance that changes from inductive to capacitive as the frequency is changed. The expression for  $L_{eq}$  is

( II. INVERTED MAGNETRON STRUCTURE )

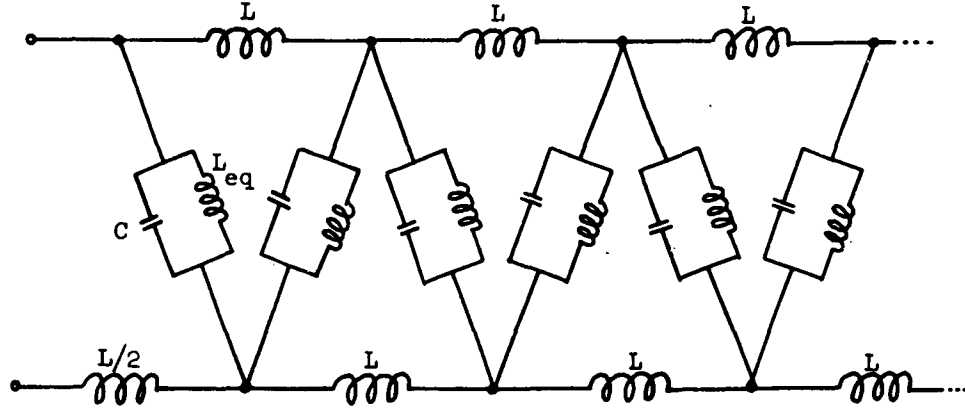


FIG. 8.--Equivalent circuit for the structure of Fig. 1.

$$L_{eq} = \frac{-1}{\omega^2 C_{eq}} = -\frac{\epsilon_0 \mu_0 R^2}{x^2 C_{eq}} = \frac{\delta \mu_0 R}{x d} \frac{J_n(x) N_n(\xi x) - N_n(x) J_n(\xi x)}{J_n'(x) N_n(\xi x) - N_n'(x) J_n(\xi x)} = \frac{\delta \mu_0 R}{x d} B_n^{-1}(x, \xi) \quad (4)$$

where  $x = 2\pi R / \lambda_0$  and  $\xi = r/R$ .

The quantity  $C$  in Fig. 8 denotes the capacitance between the bars in a length  $\Delta$  and should also contain the effect of the plate edges. In this calculation we shall include only the capacitance between the bars because the effect of the plate edges is small compared to the other terms in  $L_{eq}$ . Thus

$$C = \pi \epsilon_0 \Delta / \log \left[ \frac{d + \sqrt{d^2 - 4a^2}}{2a} \right] = C_0 \Delta \quad (5)$$

The quantity  $L$  in Fig. 8 is given approximately by

$$L = \frac{\epsilon_0 \mu_0}{C} \quad (6)$$

The circuit of Fig. 8 is a lumped continuous transmission line made up of elementary four-terminal networks such as shown in Fig. 9. The reactance

( II. INVERTED MAGNETRON STRUCTURE )

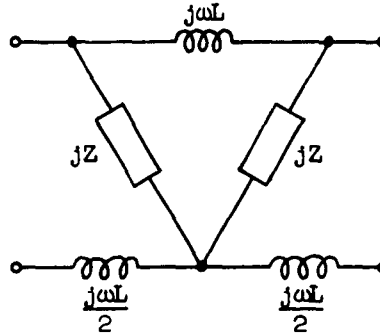


FIG. 9.--Four-terminal network elements of the line of Fig. 8.

Z is given by

$$Z = \omega L_{eq} / (1 - \omega^2 C L_{eq}) = \omega L_{eq} / [1 - (C/C_{eq})] \quad (7)$$

The characteristic impedance  $Z_c$  and the phase delay  $\beta$  of the wave propagating along the bars can be expressed in terms of the open-circuit and short-circuit impedance of the transmission line:

$$Z_c = \pm \sqrt{Z_o Z_s}$$

$$\cos \theta = \cos \beta \Delta = \pm [1 - (Z_s/Z_o)]^{-1/2}$$

where

$$Z_o = j \frac{2A^2 + 4Z\omega L + \omega^2 L^2}{2(2Z + \omega L)}$$

$$Z_s = j \frac{\omega L(2Z + \omega L)(4Z + \omega L)}{2(2Z^2 + Z\omega L + \omega^2 L^2)} \quad (8)$$

Equation (8) is a good approximation for the  $n = 0$  mode; however, it is not a good approximation for higher-order modes because of the voltage variation along the circumference of the plates.

From Eqs. (4) through (8) the phase characteristic diagram and the characteristic impedance as a function of frequency have been calculated approximately for the structure shown in Fig. 6. The results of this calculation are shown in Fig. 10, where the  $n = 0$  ( $TM_{001}$  and  $TM_{002}$ ) and the  $n = 1$  ( $TM_{011}$ ) modes are shown. The frequency  $f$  is the ordinate and the abscissa

(II. INVERTED MAGNETRON STRUCTURE )

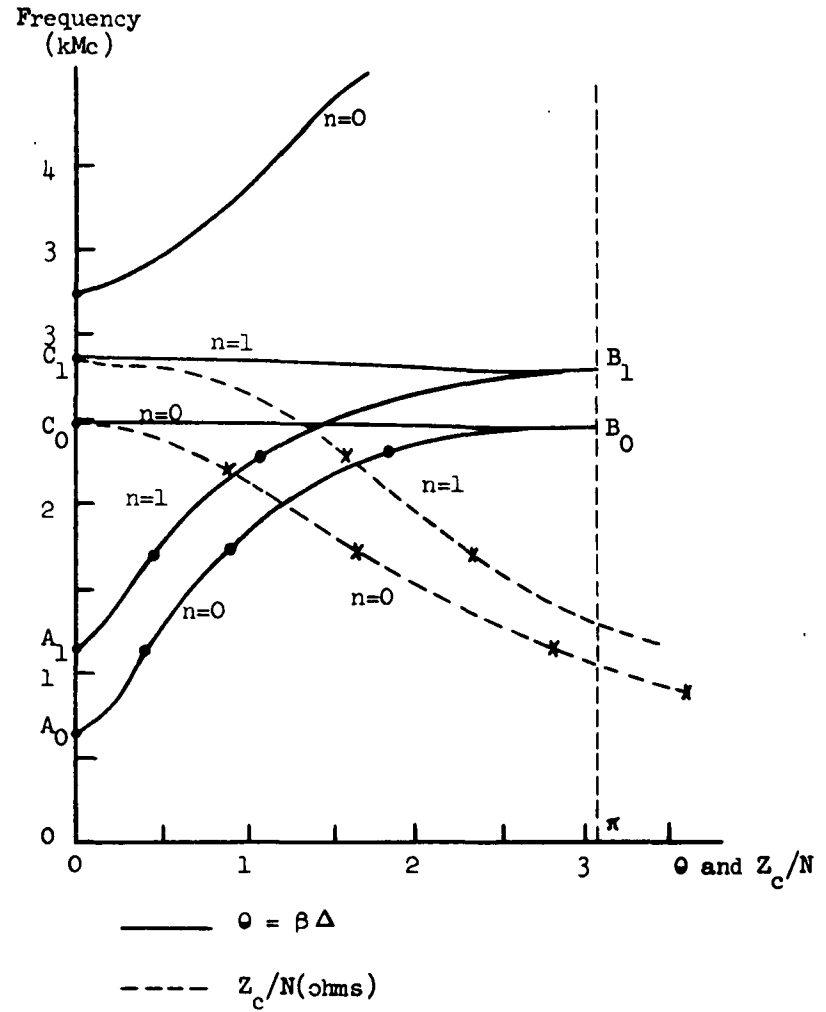


FIG. 10.--Phase characteristics and characteristic impedance for the structure of Fig. 6.



(II. INVERTED MAGNETRON STRUCTURE)

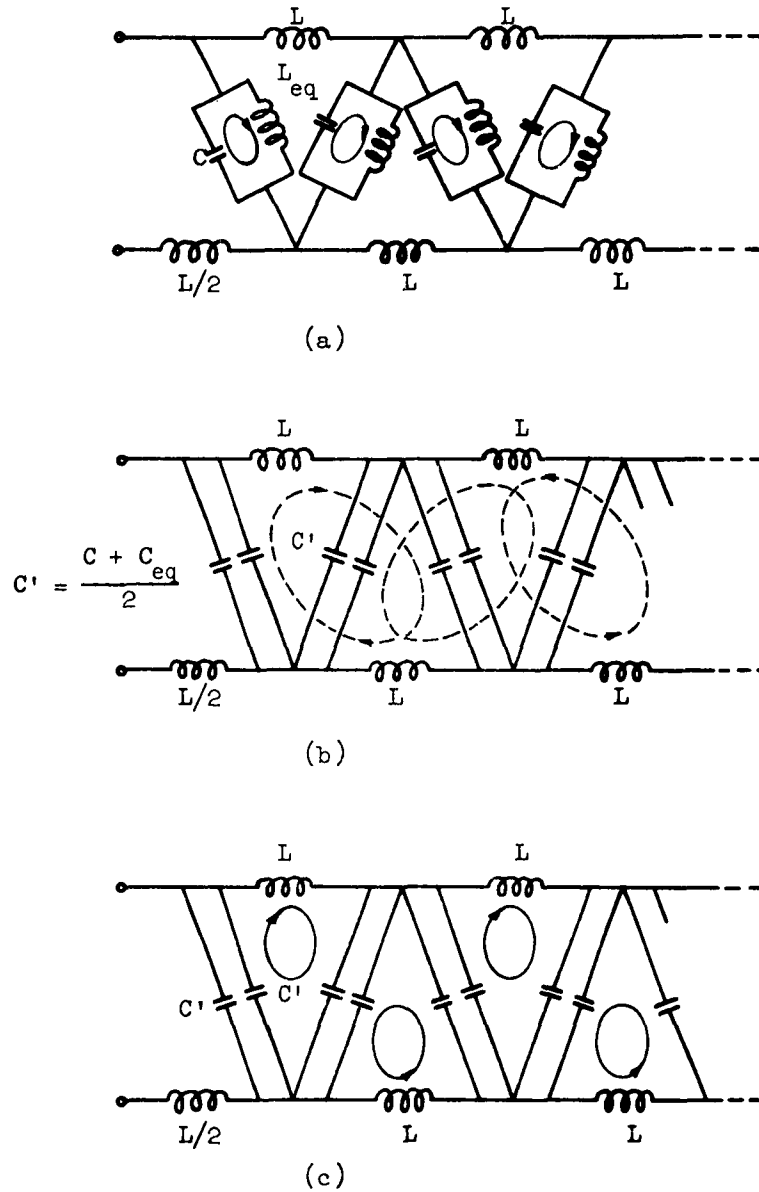


FIG. 11.--Equivalent-circuit representation for various resonant conditions: (a) parallel resonance, (b) series resonance, (c) combined resonance.

## (II. INVERTED MAGNETRON STRUCTURE)

is  $\theta = \beta\Delta$ . Also on the abscissa is the characteristic impedance  $Z_c$  divided by the number of bars  $N$  (here, 60).

The points  $A_0$  and  $A_1$  denote the conditions where the wave velocity along the bars is zero and  $C$  and  $L_{eq}$  have the value corresponding to parallel resonance for each mode (Fig. 11a). The points  $B_0$  and  $B_1$  are at the place where the conditions for series resonance exist (Fig. 11b). Two groups of circuit elements are possible for such series circuit, as shown in Fig. 11b by the solid and dotted lines. The points  $C_0$  and  $C_1$  are another resonant condition that can occur for each mode (Fig. 11c). The phase difference per section is  $\pi$  in Fig. 11b and  $2\pi$  or zero in Fig. 11c.

The resonances of the structure of Fig. 6 are easily determined from the result shown in Fig. 10. Since seven main cavities are used, the resonant conditions are given by  $\beta\Delta = q\pi/7$ , where  $q$  is an integer. Thus, from Fig. 10,  $f = 1250$  Mc for  $q = 1$  and  $f = 1755$  Mc for  $q = 2$  for the  $n = 0$  mode. These frequencies are a little higher than the lowest cutoff frequency for the  $n = 1$  mode, which explains the spectrum of Fig. 7.

### E. CAVITY LOSSES AND Q

In this section we shall obtain an estimate of the value of  $Q$  for the unit cavity and the distribution of losses along the cavity surface, assuming the bars to be absent. The power dissipated per unit area is given by

$$\sigma_p = \frac{R_s}{2} \left( \frac{k_0 E_0}{\omega_0 \mu_0} \right)^2 \left[ J_1(k_0 \rho) - \frac{J_0(k_0 r)}{N_0(k_0 r)} N_1(k_0 \rho) \right]^2 \quad (9a)$$

$$\sigma_a = \frac{R_s}{2} \left( \frac{k_0 E_0}{\omega_0 \mu_0} \right)^2 \left[ J_1(k_0 r) - \frac{J_0(k_0 r)}{N_0(k_0 r)} N_1(k_0 r) \right]^2$$

The maximum value of the time-average stored energy density is given by

$$\sigma_m = \frac{\mu_0}{2} \frac{k_0 E_0}{\omega_0 \mu_0} \left[ J_1(k_0 \rho) - \frac{J_0(k_0 r)}{N_0(k_0 r)} N_1(k_0 \rho) \right]^2 \quad (9b)$$

The surface resistance is

$$R_s = \frac{\omega \mu}{2\sigma}$$

where  $\sigma$  is the conductivity of the cavity material.

( II. INVERTED MAGNETRON STRUCTURE )

Total power dissipated in the structure is given by

$$P_L = 2 \int_r^R 2\pi \rho \sigma_p d\rho + 2\pi r \delta \sigma_a \quad (10)$$

The total stored energy is

$$\bar{W}_s = \int_r^R 2\pi \rho \sigma_m d\rho$$

Using the relation between the constant  $E_0$  and the voltage at the gap  $V_0$  (Fig. 12)

$$E_0 = \frac{V_0}{\delta} \left[ J_0(k_0 R) - \frac{J_0(k_0 r)}{N_0(k_0 r)} N_0(k_0 r) \right]^{-1}$$

we can determine the cavity losses from (9a) and determine the cavity Q from

$$Q = \frac{\omega_0 W}{P_L} \quad (11)$$

Taking the conductivity of copper as  $10^8$  mhos/m, we have for the cavity Q

$$\frac{1}{Q} = 8.26 \times 10^{-6} \frac{\sqrt{R}}{\delta} + 18.8 \times 10^{-6} \frac{1}{\sqrt{R}} \quad \text{for } \xi = \frac{r}{R} = \frac{1}{4}$$

$$\frac{1}{Q} = 9.18 \times 10^{-6} \frac{\sqrt{R}}{\delta} + 20.7 \times 10^{-6} \frac{1}{\sqrt{R}} \quad \text{for } \xi = \frac{1}{6}$$

If we use the values  $R = 60$  mm and  $\delta = 1.5$  mm

$$Q = 697 \quad (\xi = 1/4)$$

$$Q = 636 \quad (\xi = 1/6)$$

The distributions of losses on the plate surfaces are shown in Fig. 13 where the small contribution from  $\sigma_a$  has been neglected.

The expressions for the total losses can be simplified as follows

$$P_L = \left( 3.06 \times 10^{-8} \frac{R^{3/2}}{\delta^2} + 6.92 \times 10^{-8} \frac{\sqrt{R}}{\delta} \right) V_0^2 \quad (\xi = 1/4)$$

and

$$P_L = 3.69 \times 10^{-8} \frac{R^{3/2}}{\delta^2} + 8.33 \times 10^{-8} \frac{\sqrt{R}}{\delta} V_0^2 \quad (\xi = 1/6)$$

For a value  $V_0 = 5000$  v and the same dimensions ( $R = 60$  mm and  $\delta = 1.5$  mm),

( II. INVERTED MAGNETRON STRUCTURE )

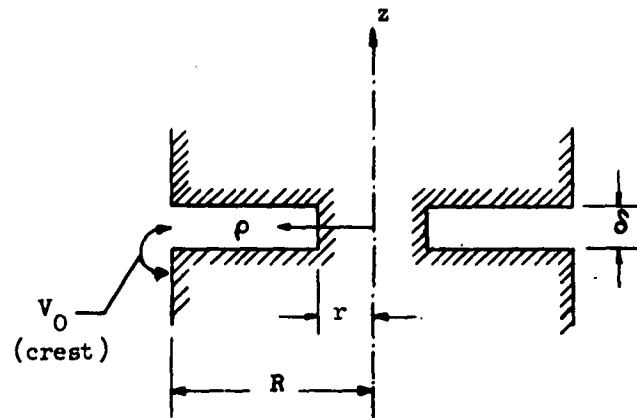


FIG. 12.--Schematic representation of gap.

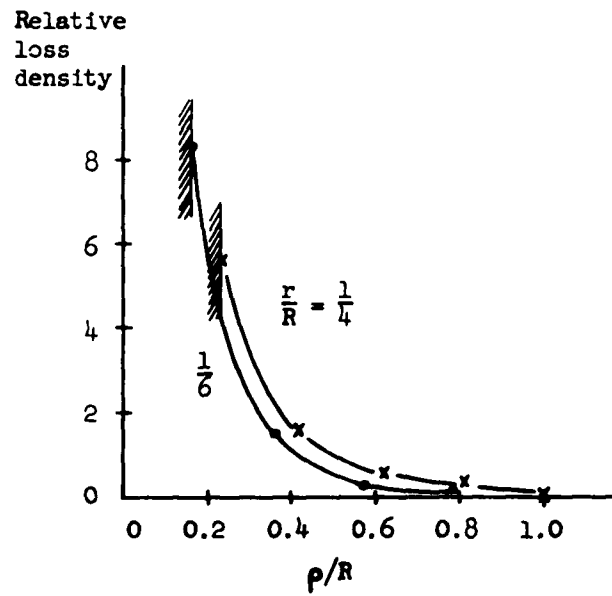


FIG. 13.--Distribution of loss density.

## (II. INVERTED MAGNETRON STRUCTURE )

$$P_L = 4990 + 283 w \quad (\xi = 1/4)$$

$$P_L = 6010 + 340 w \quad (\xi = 1/6)$$

The first loss term is the plate loss and the second the losses on the cylindrical portion ( $\rho = r$ ).

From Fig. 13 it is obvious that the losses are largest near the central cylinder. This may present a difficult problem for cooling a high-power magnetron structure. The problem will be worst for small values of  $\xi$ , which give good mode separation.

### F. MODE-SEPARATION IMPROVEMENT

Mode separation can be improved by changing the gap length as a function of radius, as shown in Fig. 14, since the frequency for each mode changes differently from the uniform-gap case.

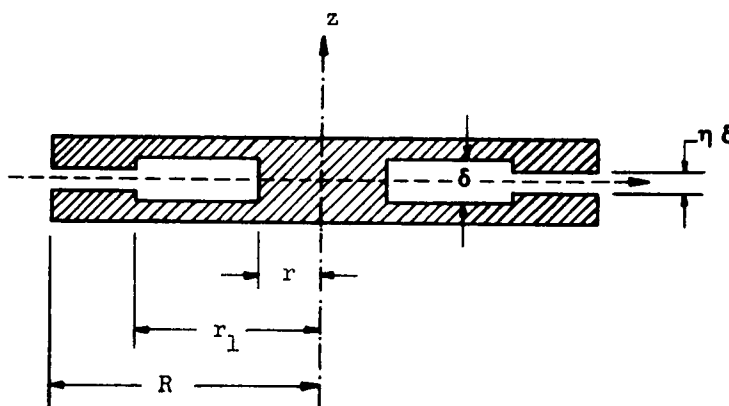


FIG. 14.--Gap modified for improved mode separation.  $r/R = \xi$ ,  $r_1/R = \xi_1$ ,  $\delta \ll r$ .

We assume as approximate boundary conditions for the  $TM_0$  mode

$$\left. \begin{aligned} \delta E_z &= \eta \delta E_{z1} \\ I_\rho &= I_{\rho 1} \\ I_{\rho 1} &= 0 \end{aligned} \right\} \quad \begin{aligned} &\text{at } \rho = r_1 \\ &\text{at } \rho = R \end{aligned} \quad (13)$$

where the subscript 1 denotes the region  $r_1 < \rho < R$ .

The expressions for the electric and magnetic field are similar to Eqs. (1) and (2). The characteristic equations for the cavity resonance are

## (II. INVERTED MAGNETRON STRUCTURE)

$$\frac{J_n'(x)}{N_n'(x)} = \frac{\eta J_n(\xi_1 x) \alpha - J_n'(\xi_1 x) \beta}{\eta N_n(\xi_1 x) \alpha - N_n'(\xi_1 x) \beta} \quad (14)$$

where

$$\alpha = J_n'(\xi_1 x) N_n(\xi x) - J_n(\xi x) N_n'(\xi_1 x)$$

$$\beta = J_n(\xi_1 x) N_n(\xi x) - J_n(\xi x) N_n(\xi_1 x)$$

and  $x = kR$ . It is easily seen that Eq. (14) reduces to (2b) for  $\eta = 1$  and  $k = 0$ .

For the case  $\xi = 1/8$  and  $\xi_1 = 6/8$ , the resonant frequencies for the  $n = 0$  and  $n = 1$  modes were calculated from Eq. (14) as a function  $n$ . These results, which are given in Fig. 15, show that a better mode separation is obtained for small  $\eta$ .

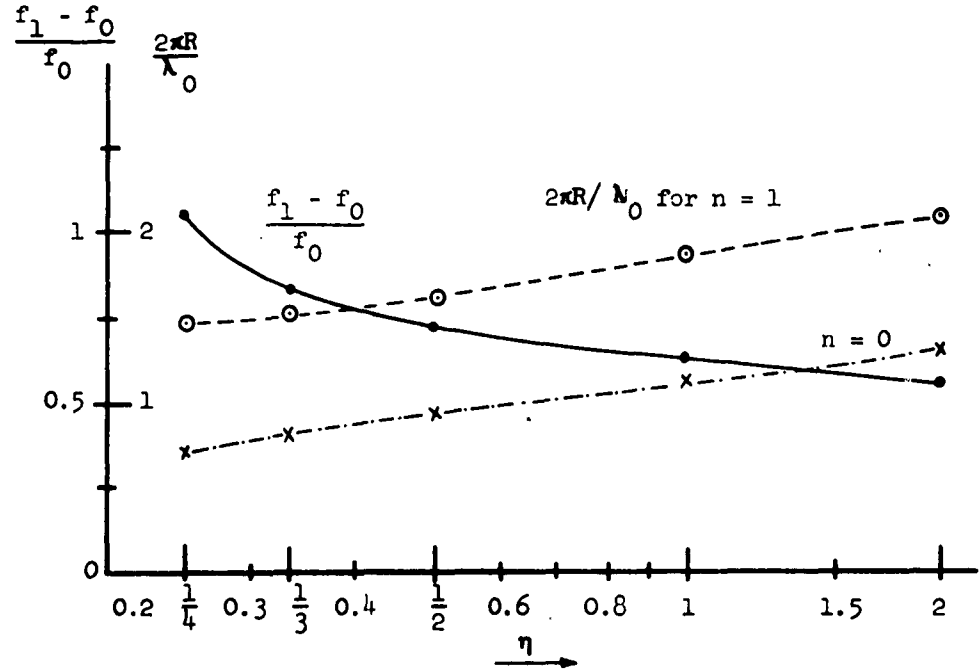


FIG. 15.--Calculation of resonant frequency from Eq. (14) with  $\xi = 1/8$  and  $\xi_1 = 6/8$ .

### III. CONVENTIONAL-MAGNETRON ANODE STRUCTURE

#### A. ANODE STRUCTURE, SYMBOLS, AND DEFINITIONS

In this section we shall analyze the rf properties of structures such as shown in Figs. 16 and 17. These configurations are of a conventional magnetron design where the anode is the outer structure. The configuration shown in Fig. 16 is a cylindrical one, similar to that analyzed in Sec. II. The configuration shown in Fig. 17 is suitable for a linear magnetron amplifier. A direct current flowing along the central structure can produce a dc magnetic field, so that electrons move in the axial direction owing to both dc electric and magnetic fields.

#### B. RESONANT FREQUENCY OF AN INDIVIDUAL CAVITY

Following the analysis given in Sec. II the resonant frequency for a unit cavity is calculated with the assumption of uniform capacitive loading to replace the effects of the bars and the edges at the inner opening. The resonant frequency is determined from the following formula:

$$B_n(x, \xi) = \frac{J_n'(x)N_n(\xi x) - N_n'(x)J_n(\xi x)}{N_n(x)J_n(\xi x) - J_n(x)N_n(\xi x)} = \frac{\kappa \delta}{\epsilon_0 r} x \quad (15)$$

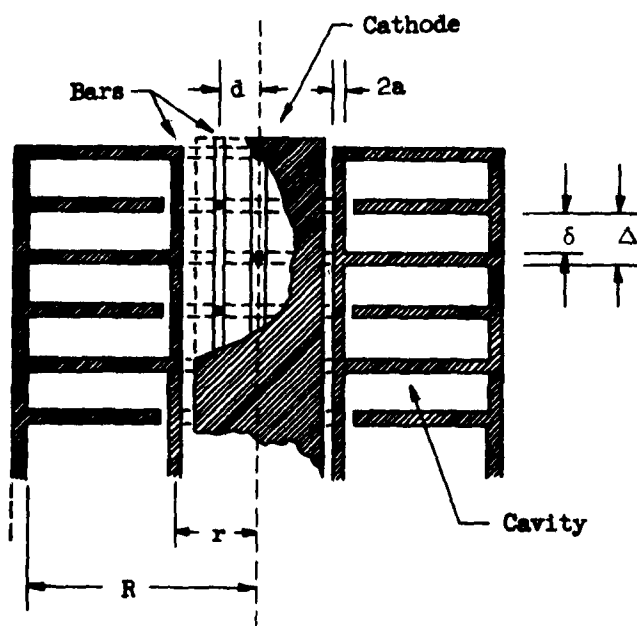
where  $x = kr = 2\pi r/\lambda_0$ ,  $\xi = R/r$ , and  $\kappa$  is given by the same expression as in Eq. (3). For  $k = 0$ , the resonance condition is given simply by

$$J_n'(x)N_n(\xi x) = N_n'(x)J_n(\xi x) \quad (16)$$

The solutions of Eq. (16) for  $n = 0$  and  $n = 1$  modes are shown in Fig. 18. The mode separation is better for high values of  $\xi$ . However, this means a smaller value of  $r$  for a particular  $R$  value, and therefore the interaction space for the electron beam is limited.

Figure 19 gives the relation between  $r\xi$  and the rate of mode separation for a fixed resonant frequency. For comparison with Fig. 4, Fig. 18 is also replotted in terms of  $kR$  instead of  $kr$  and  $\xi = (r/R)$  instead of  $\xi = (R/r)$ . The resonant frequency of a cavity for a given value of outer radius and inner to outer radius ratio are much higher and the interaction space is smaller.

21.  
(III. OUTER-ANODE STRUCTURE)



CI FIG. 16.--Structure for cylindrical magnetron.

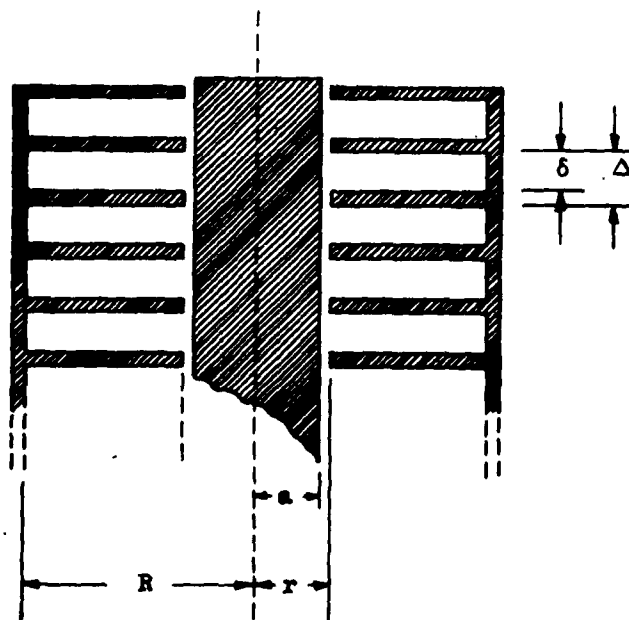


FIG. 17.--Structure for linear magnetron.



(III. OUTER-ANODE STRUCTURE)

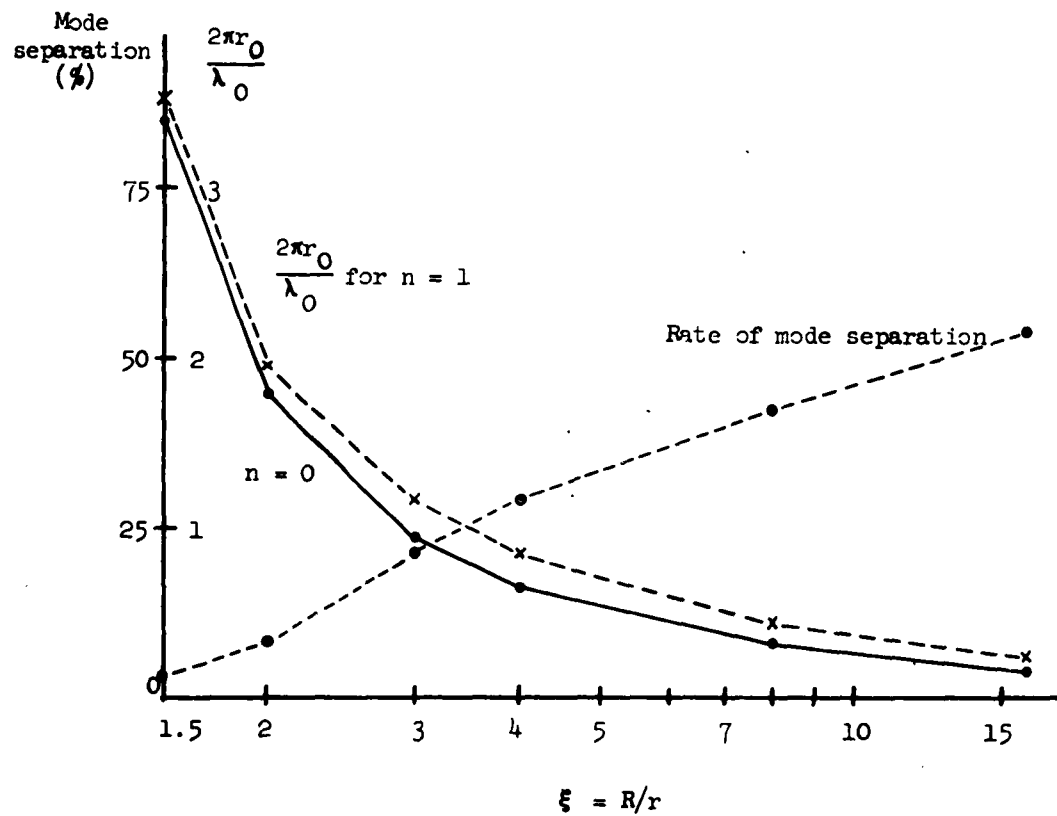


FIG. 18.--Solutions of Eq. (18) for  $\kappa = 0$ .

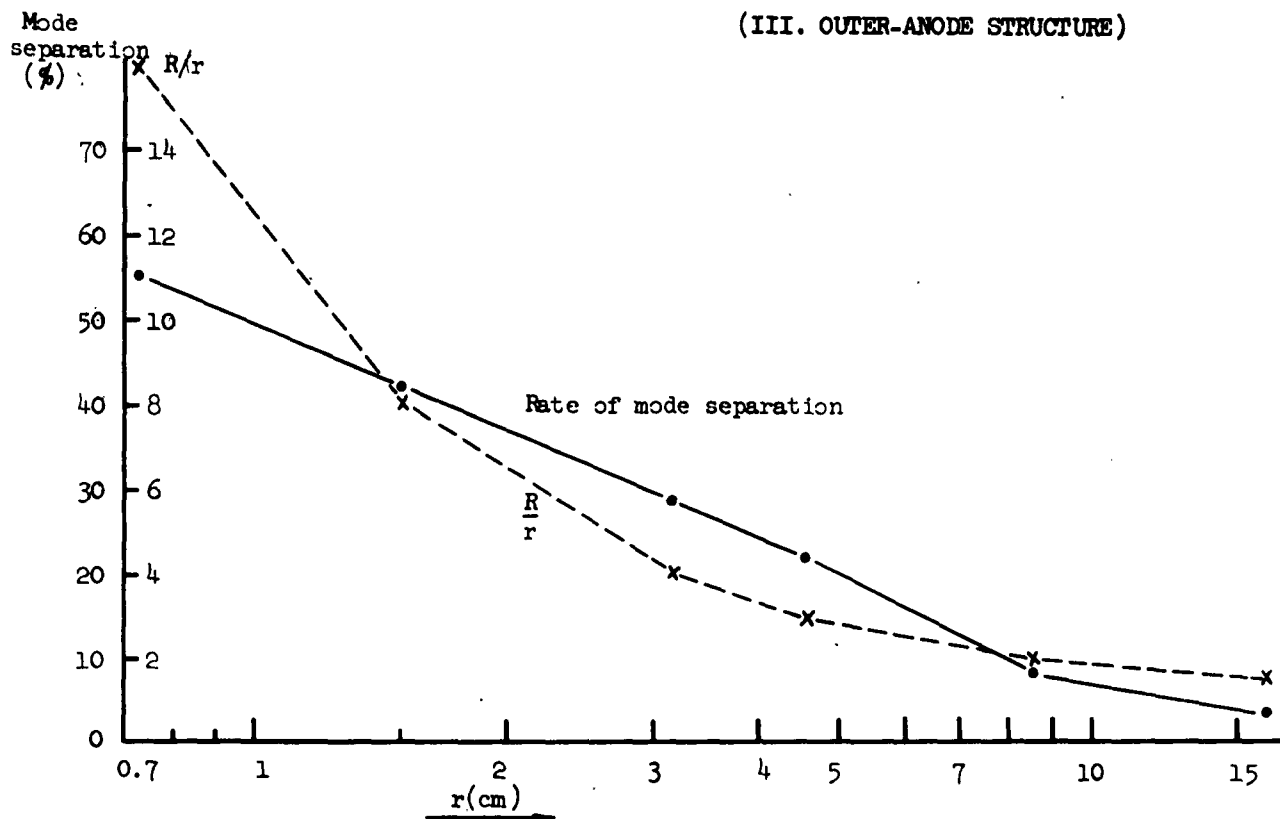
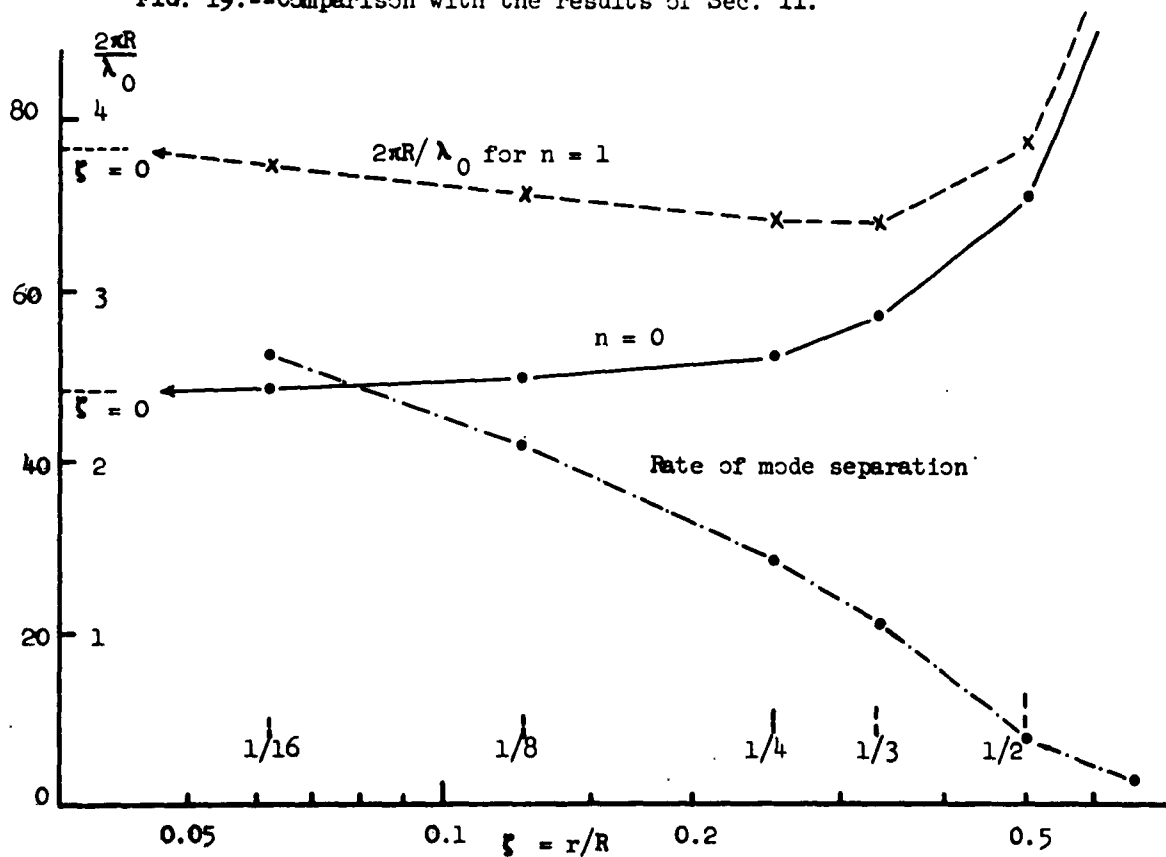


FIG. 19.--Comparison with the results of Sec. II.



### (III. OUTER-ANODE STRUCTURE)

#### C. MEASUREMENT OF RESONANT FREQUENCIES

Figure 20 is a schematic diagram of the experimental setup used to test the theory presented in this analysis. Table 3 is a tabulation of the measured results compared with the theoretically calculated values of resonant frequency.

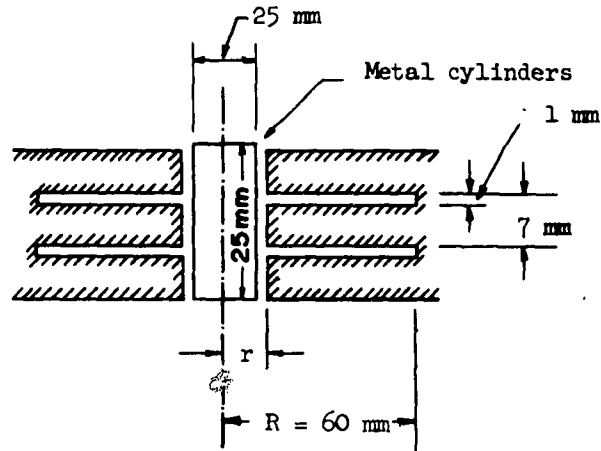


FIG. 20.--Test configuration.

Table 3.--Resonant frequencies (in megacycles) for the structure of Fig. 20.

r (mm)	n = 0 mode		n = 1 mode		Note	Mode separation(%)
	Measured	Calculated	Measured	Calculated		
6	1935	1980	2980	2900	No metal cylinder	54
10	1975,1968	2055	2915,2900	2830	"	> 46.8
12.5	2017,2027	2080	2820,2845	2810	"	> 39.8
15.7	2082,2099	2105	2765,2793	2790	"	> 31.7
15.7	1920,2082	-	2768,2800	-	With metal cylinder	> 37.6
15.7	1865,2070	-	2785,2855	-	"(somewhat eccentric)	-

### (III. OUTER-ANODE STRUCTURE)

Measured values for the structure are in good agreement with the critically calculated values. The metal cylinder has little effect on the resonant frequency because of the capacity it introduces. The next step in the measurements was to investigate the effect of a small number of connecting bars. The results of these measurements are tabulated in Table 4. It was expected that the addition of the bars would reduce the  $n = 0$  mode frequency and improve the mode separation; however, the addition of the bars did not produce this result as may be seen from a comparison of Parts A and B of Table 4.

If a metal shaft is inserted along the axis, it is expected to produce the same effect as the bars insofar as their influence on the mode can be included in the equivalent capacitance. According to Table 4 the mode separation is worse with the shaft in place whenever the value of  $R/r$  is less than 4 or 5, and the mode separation is better if this ratio is larger. The resonant frequency calculated for a Type C structure in Table 4 assumes no capacitive loading and gives  $f_0 \approx 2500$  Mc and  $f_1 \approx 3380$  Mc. The capacitance of the bars is thus seen to cause a considerable reduction in the resonant frequency. The  $Q$  of some of the cavities was measured approximately from the resonant curves. The  $Q$  for smaller gap lengths was found to be the order of hundreds and for larger gap lengths, of the order of 1000.

#### D. EQUIVALENT CIRCUITS FOR LINEAR MAGNETRON STRUCTURE

The equivalent circuit for the structure shown in Fig. 16 is the same as that given in Fig. 8. The equivalent loading reactance in this case is

$$L_{eq} = \frac{-1}{\omega^2 C_{eq}} = \frac{\delta \mu_0 r}{\omega^2 x d} B_n^{-1}(x, \xi) \quad (17)$$

Since the circuit is the same, similar phase characteristics for the two cases are expected.

The analysis will be carried out for the linear magnetron structure shown in Fig. 17.

1. ANALYSIS FOR  $n = 0$  MODE. Figure 21 gives the equivalent circuit with the gap length assumed to be much smaller than a wavelength. The equivalent inductance for a unit cell is

$$L_{x0} = \frac{\mu_0 \delta}{2\pi x} B_0^{-1}(x, \xi) \quad (18)$$

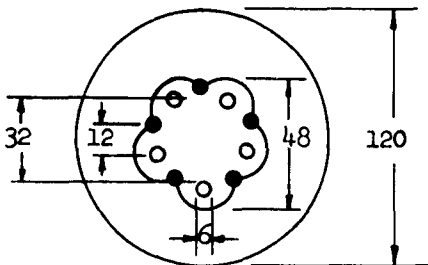
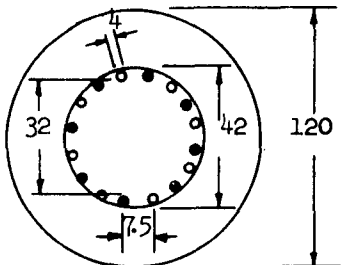
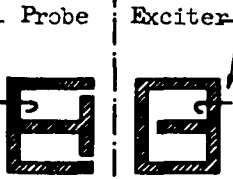
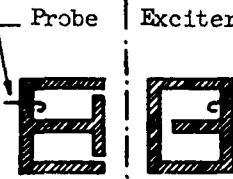
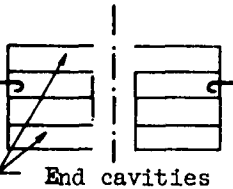
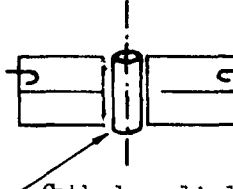
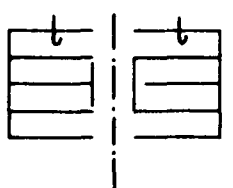
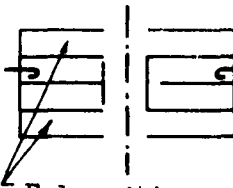
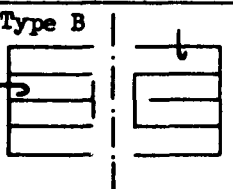
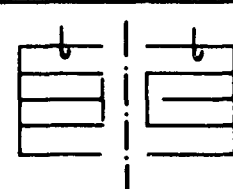
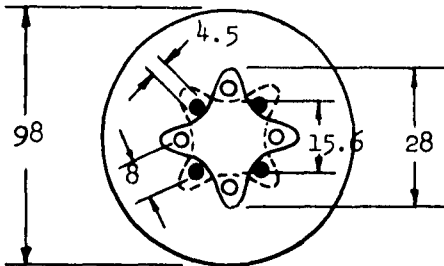
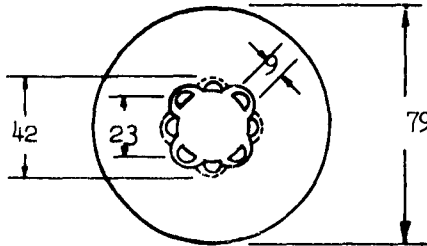
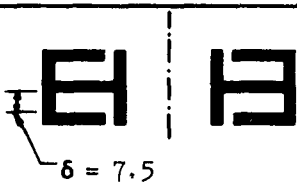
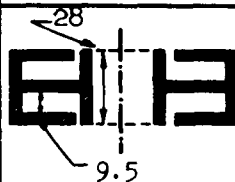
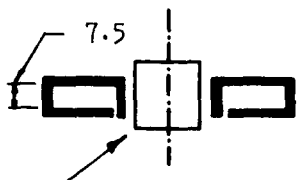
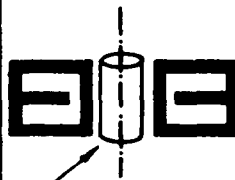

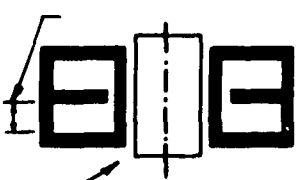
Table 4.--Resonant frequencies measured with structures with bars				
	Type A		Type B	
Schematic view of the structure (all dimensions in millimeters)	 <p><math>R/r \approx 3, \delta = 1.5, \Delta = 7.5</math></p>		 <p><math>R/r \approx 3, \delta = 1.5, \Delta = 7.5</math></p>	
	Schematic cross-section view	Frequencies measured	Schematic cross-section view	Frequencies measured
Basic measurements		$n = 0$ mode 2205 Mc $n = 1$ mode 2580 Mc $\frac{f_1 - f_0}{f_0} = 0.170$		$n = 0$ mode 1934 Mc $n = 1$ mode 2430 Mc $\frac{f_1 - f_0}{f_0} = 0.257$
Miscellaneous measurements	 <p>End cavities</p>	$n = 0$ 2055 Mc 2276 Mc $n = 1$ 2468 Mc 2692 Mc	 <p>Cathode cylinder</p>	$n = 0$ mode 1920 Mc $n = 1$ mode 2400 Mc $\frac{f_1 - f_0}{f_0} = 0.250$
	 <p>Both probes in end cavity</p>	$n = 0$ 2055 Mc (weak mode) 2155 Mc 2276 Mc $n = 1$ 2685 Mc 2700 Mc	 <p>End cavities</p>	$n = 0$ 1918 Mc 2140 Mc (faint mode) $n = 1$ 2410 Mc
	 <p>One probe in end cavity</p>	$n = 0$ 1918 Mc 2140 Mc (very strong) $n = 1$ 2405 Mc 2710 Mc	 <p>Both probes in end cavity</p>	$n = 0$ 1918 Mc (weak) 2112 Mc 2142 Mc $n = 1$ 2402 Mc (weak) 2646 Mc (weak) 2710 Mc 2726 Mc

Table 4 (Continued)

Table 4 (Continued)				
	Type C		Type D	
Schematic view of the structure (all dimensions in millimeters)				
	$R/r \approx 5, \quad \delta = 7.5 \text{ and } 12 \text{ mm}$		$R/r = 2.5, \quad \delta = 9.5 \text{ mm}$	
	Schematic cross-section view	Frequencies measured	Schematic cross-section view	Frequencies measured
Basic measurements	 $\delta = 7.5$	$f_0 = 2020 \text{ Mc}$ $f_1 = 2920 \text{ Mc}$ $\frac{f_1 - f_0}{f_0} = 0.446$	 28 9.5	$f_0 = 1490 \text{ Mc}$ $f_1 = 1896 \text{ Mc}$ $\frac{f_1 - f_0}{f_0} = 0.272$
Miscellaneous Measurements	 7.5 Cathode cylinder 13(diam.) x 13	without cylinder $f_0 = 1854 \text{ Mc}$ $\frac{f_1 - f_0}{f_0} = 0.545$ with cylinder $f_0 = 1821 \text{ Mc}$ $\frac{f_1 - f_0}{f_0} = 0.566$	 28 9.5 Cathode cylinder 21.5(diam.) x 30	$f_0 = 1386$ $f_1 = 1670$ $\frac{f_1 - f_0}{f_0} = 0.205$
	 $\delta = 12$	$f_0 = 1348 \text{ Mc}$ $f_1 = 2162 \text{ Mc}$ $\frac{f_1 - f_0}{f_0} = 0.568$	Cathode cylinder 21.5(diam.) x 50 Cathode cylinder 19(diam.) x 30	$f_0 = 1380$ $\frac{f_1 - f_0}{f_0} = 0.21$ $f_0 = 1460$ $\frac{f_1 - f_0}{f_0} = 0.243$
	 12 Cathode cylinder 13(diam.) x 28	$f_0 = 1348$ $f_1 = 2098$ $\frac{f_1 - f_0}{f_0} = 0.556$	Cathode cylinder 12.5 (diam.) x 30 Cathode cylinder 12.5 (diam.) x 30 Eccentric position	$f_0 = 1486$ $\frac{f_1 - f_0}{f_0} = 0.268$ $f_0 = 1456$ $\frac{f_1 - f_0}{f_0} = 0.237$

### (III. OUTER-ANODE STRUCTURE)

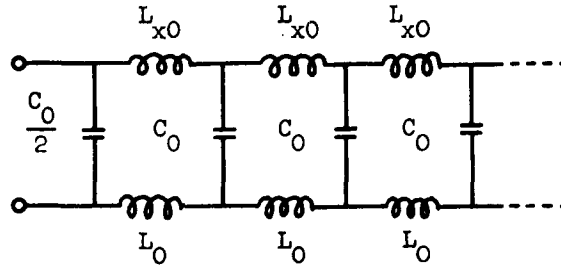


FIG. 21.--Equivalent circuit for  $n = 0$  mode.

The capacitance between cathode and anode per section is

$$C_0 = 2\pi \epsilon_0 \Delta / \log (r/a)$$

and the corresponding inductance is

$$L_0 = \frac{\mu_0 \Delta}{2\pi} \log (r/a) \quad (19)$$

The phase characteristics for waves propagating in the axial direction are given by

$$\cos \theta = 1 - \frac{\chi}{2} \quad (20)$$

where  $\beta \Delta = \theta$  and  $\chi = \omega^2 V_0 (L_0 + L_{x0})$ . The characteristic admittance is

$$Y_{ch} = \omega C_0 \sqrt{\frac{4}{\chi} - 1} \quad (21)$$

2. ANALYSIS FOR  $n = 1$  MODE. A good equivalent circuit representation is more difficult to obtain in this because of the field distribution. An equivalent circuit that is a good approximation to the structure is shown in Fig. 22. The quantity  $\omega_c$  is the resonant frequency of the TE coaxial line mode and is given by the first root of

$$\frac{J_1'(ka)}{J_1'(kr)} = \frac{N_1'(ka)}{N_1'(kr)} \quad (22)$$

where

$$k = 2\pi/\lambda_0 = \omega_c \sqrt{\mu_0 \epsilon_0}$$

The effective capacitance  $C_1$  is determined from the electric stored energy:

(III. OUTER-ANODE STRUCTURE)

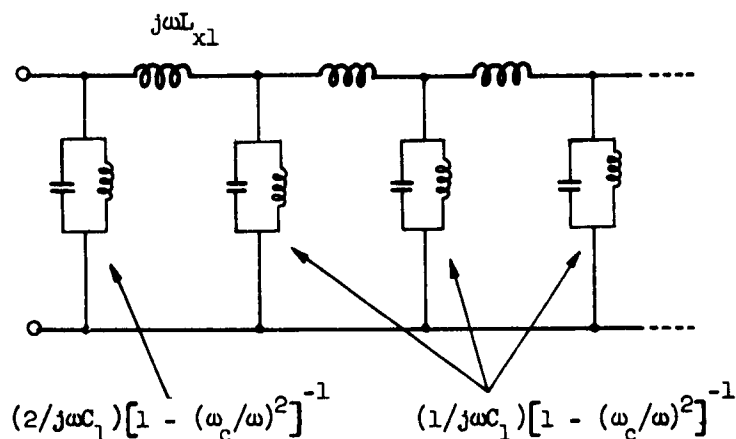


FIG. 22.--Equivalent circuit for the  $n = 1$  mode.

$$\frac{1}{2} C_1 V_1^2 = \int \frac{\epsilon_0 E_1^2}{2} dv \quad (23)$$

so that

$$C_1 \approx \pi \epsilon_0 (\Delta - \delta)/2 \log(r/a)$$

where  $V_1$  and  $E_1$  are respectively the voltage and field between the anode and cathode for the  $n = 1$  mode. The circuit of Fig. 22 has its cutoff at  $\omega_c^3$

The effective inductance can also be determined from energy considerations:

$$L_{x1} = \frac{\pi \epsilon_0 \delta}{8x} B_1^{-1}(x, \xi) \quad (24)$$

The propagation characteristics of the circuit are given by

$$\cos \theta = 1 - \frac{\chi}{2} \quad (25)$$

where  $\theta = \beta \Delta$  and  $\chi = \omega^2 L_{x1} C_1 [1 - (\omega_c/\omega)^2]$

The characteristic admittance is

$$Y_{ch} = \omega C_1 [1 - (\omega_c/\omega)^2] \sqrt{\frac{4}{\chi} - 1} \quad (26)$$

3. NUMERICAL RESULTS AND EXPERIMENT. The phase characteristics and the characteristic admittances for the  $n = 0$  and  $n = 1$  modes for the



### (III. OUTER-ANODE STRUCTURE)

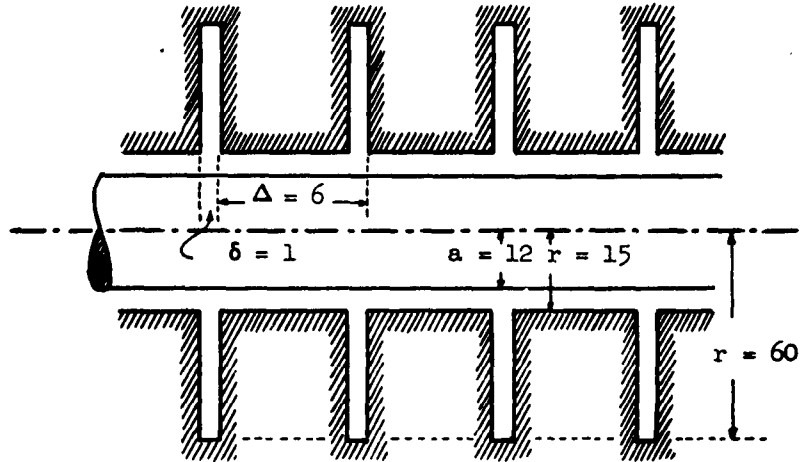


FIG. 23.--Experimental configuration.

structure shown schematically in Fig. 23 are shown in Fig. 24 for the case  $\xi = R/r = 4$ . These results were obtained by using Eqs. (17) through (26) and the impedance for the mode from these equations is the order of a few tens of ohms.

Selecting an axial length of  $q \Delta$ , where  $q$  denotes the total number of sections, we can predict all the resonances of this structure from the phase characteristic diagram of Fig. 24. Table 5 gives the results between calculated and measured resonant frequencies for a structure having six sections. As can be seen there is good agreement between the calculated and measured values of the resonant frequency. Not every frequency was measured because of superposition of some modes or difficulty of excitation of some modes.

#### E. CAVITY LOSSES AND Q

Following the analysis of Sec. II, we find the approximate Q of the structure shown in Fig. 25 from

$$\frac{1}{Q} = 12.6 \times 10^{-6} \sqrt{\frac{r}{\delta}} + 3.21 \times 10^{-6} \frac{1}{\sqrt{r}} (\xi = 4)$$

and

$$\frac{1}{Q} = 10.6 \times 10^{-6} \sqrt{\frac{r}{\delta}} + 3.99 \times 10^{-6} \frac{1}{\sqrt{r}} (\xi = 3)$$

(III. OUTER-ANODE STRUCTURE)

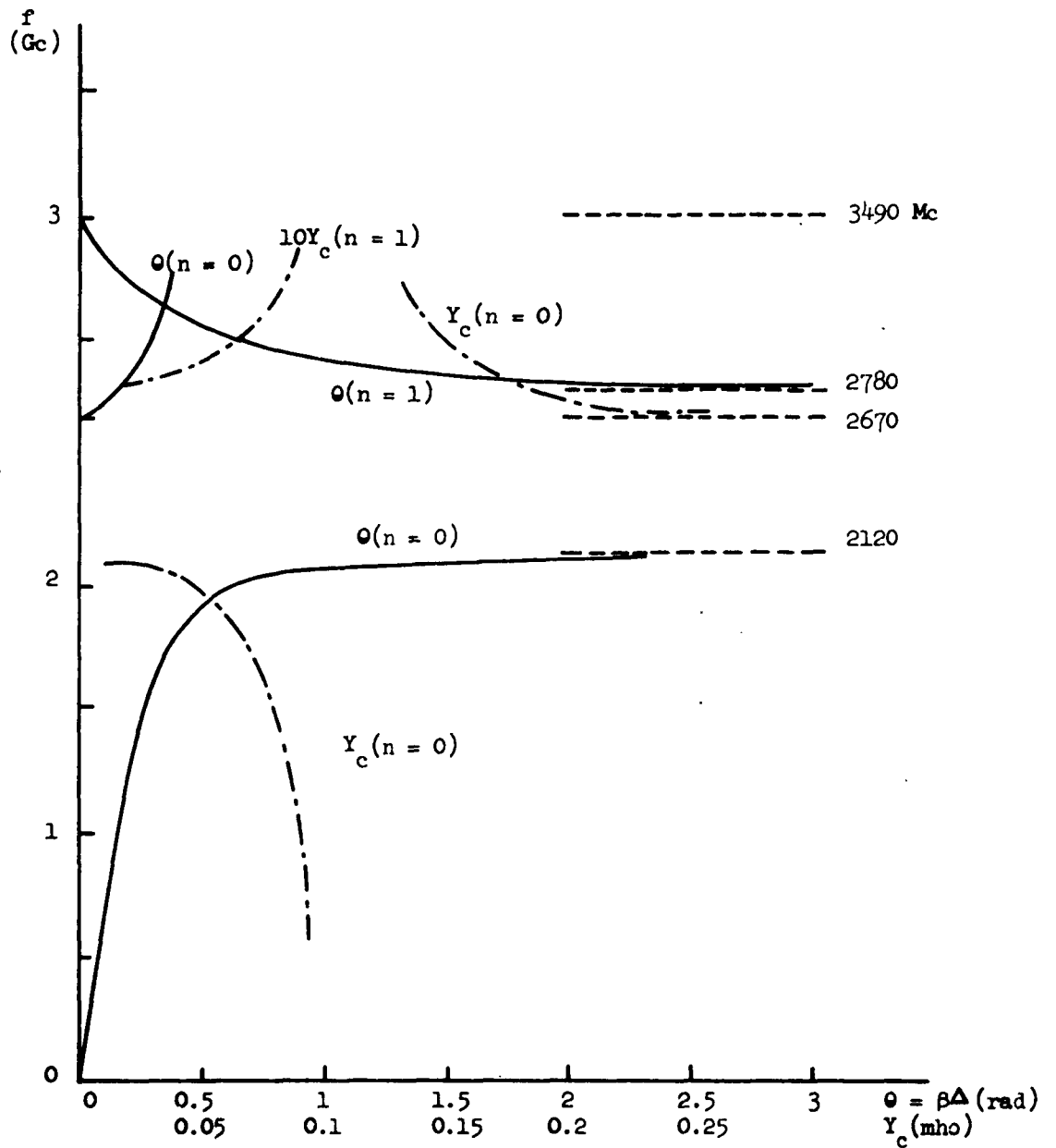


FIG. 24.--Summary of experimental results.  $R/r = 4$ ,  $r = 15$ ,  $a = 12$ ,  $\Delta = 6$ ,  $\delta = 1$  mm.

(III. OUTER-ANODE STRUCTURE)

Table 5.--Calculated and measured frequencies (in megacycles).

$r = 15 \text{ mm}$ ,  $R/r = 4$ ,  $a = 12 \text{ mm}$ ,  $\Delta = 6 \text{ mm}$ ,  $\delta = 1 \text{ mm}$ ,  $q = 6$

$n = 0$		$n = 1$	
Calculated	Measured	Calculated	Measured
2120	2091	2780	2763
2120	2078	2780	2769
2110	2041	2800	2785
2100	1922	2830	2813
2075		2890	
1930		3030	

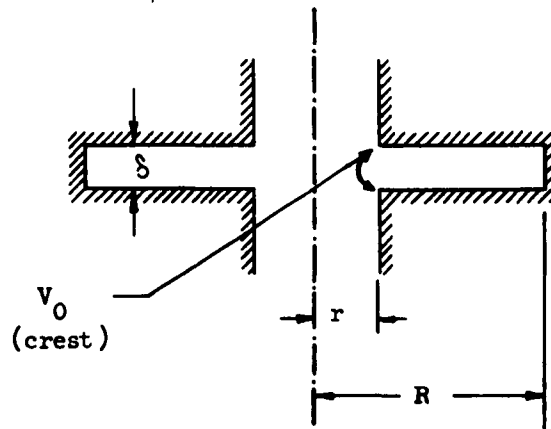


FIG. 25.--Schematic representation of gap.

Taking  $R = 60 \text{ mm}$  and  $\delta = 1.5 \text{ mm}$  we have

$$Q = 945 \quad (\xi = 4)$$

$$Q = 976 \quad (\xi = 3)$$

These  $Q$  values are about 50 per cent higher than those of the structures analyzed in Sec. II. However, for the same resonant frequency and same  $r/R$ , the  $Q$ 's in the two cases are about the same.

The total losses for this structure are

(III. OUTER-ANODE STRUCTURE)

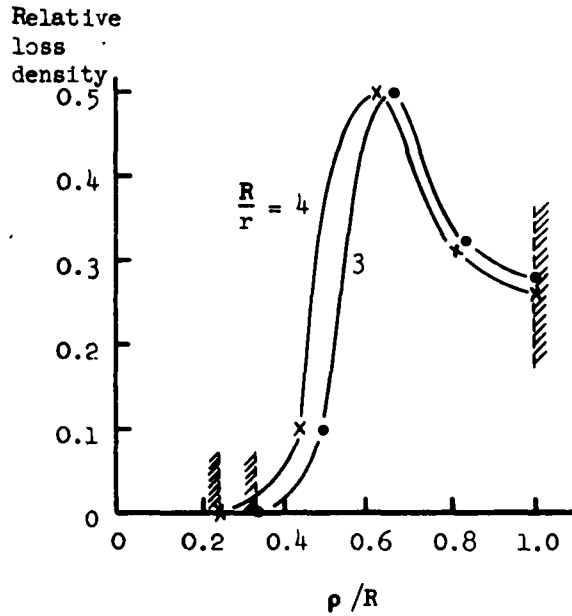


FIG. 26.--Loss-density distribution over plate surface.

$$P_L = \left( 21.0 \times 10^{-8} \frac{r^{3/2}}{\delta^2} + 5.32 \times 10^{-8} \frac{\sqrt{r}}{\delta} \right) V_0^2 \quad (\xi = 4)$$

$$P_L = \left( 14.3 \times 10^{-8} \frac{r^{3/2}}{\delta^2} + 5.36 \times 10^{-8} \frac{\sqrt{r}}{\delta} \right) V_0^2 \quad (\xi = 3)$$

Again we take  $V_0 = 5000$  v,  $R = 60$  mm, and  $\delta = 1.5$  mm:

$$P_L = 4270 + 109 w \quad (\xi = 4)$$

$$P_L = 4430 + 126 w \quad (\xi = 3)$$

Although these losses are smaller than the values of Sec. II, it must be noted that they would be larger if the frequency was the same as for structure of Sec. II.

Figure 26 gives the distribution of losses over the surfaces of the plates.

(III. OUTER-ANODE STRUCTURE)

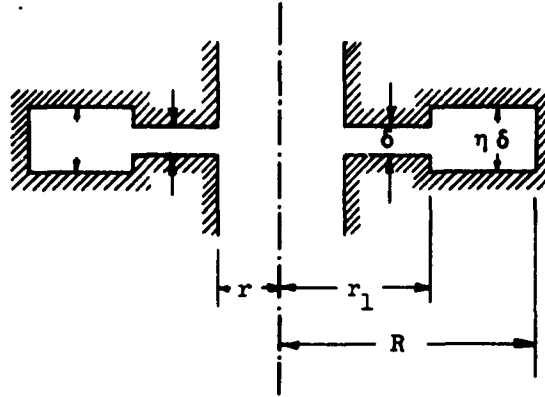


FIG. 27.--Structure used for mode-separation improvement.  
( $\xi = R/r$ ,  $\xi_1 = r_1/r$ ,  $\delta < r$ .)

F. IMPROVEMENT OF MODE SEPARATION

The method of Sec. II has been applied to the structure depicted in Fig. 27. The equations for determining the resonant frequency for various values of  $\xi$  and  $\eta$  are

$$\frac{J_n'(x)}{N_n'(x)} = \frac{J_n'(\xi_1 x)\alpha - J_n(\xi_1 x)\beta}{N_n'(\xi_1 x)\alpha - N_n(\xi_1 x)\beta} \quad (27)$$

$$\alpha = J_n(\xi_1 x)N_n(\xi x) - N_n(\xi_1 x)J_n(\xi x)$$

$$\beta = J_n'(\xi_1 x)N_n(\xi x) - N_n'(\xi_1 x)J_n(\xi x)$$

where  $x = kr$ .

Table 6 gives the value of  $x$  and the mode separation for several conditions. It is seen that the mode separation is improved by a large  $\eta$ . This has the disadvantage of a small  $r$ , which may make fabrication of the structure difficult.

G. COMPARISON OF STRUCTURES OF SECS. II AND III

At a fixed frequency of 1000 Mc, the mode separation and  $R/r$  ratio is given as a function of the interaction space radius  $R_0$  in Fig. 28. We see that the mode separation is always better for the inverted magnetron structure

Figure 29 gives the mode separation and  $R/r$  ratio as a function of the

(III. OUTER-ANODE STRUCTURE)

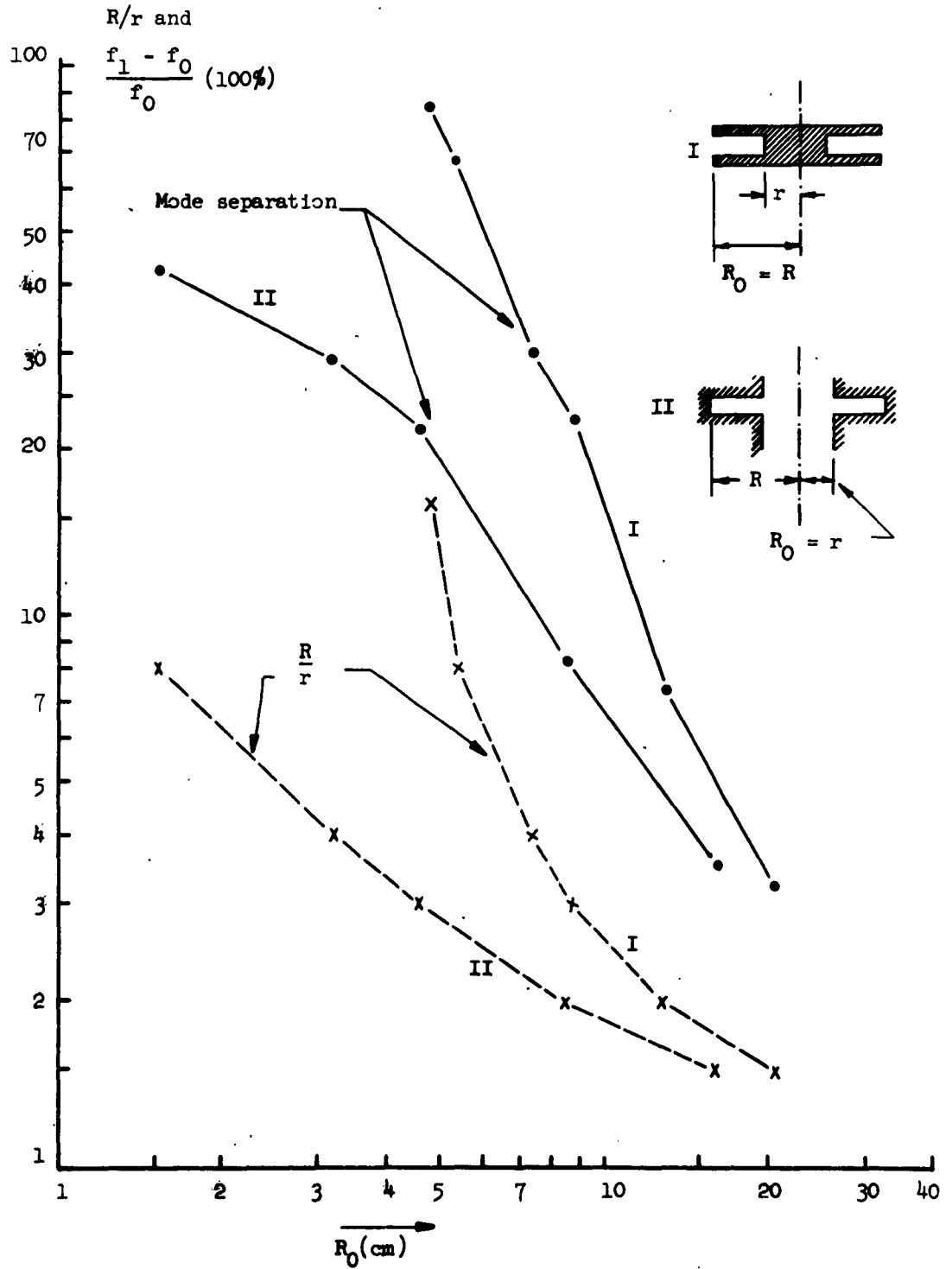


FIG. 28.--Mode separation and  $R/r$  ratio at 1000 Mc as a function of  $R_0$ .

(III. OUTER-ANODE STRUCTURE)

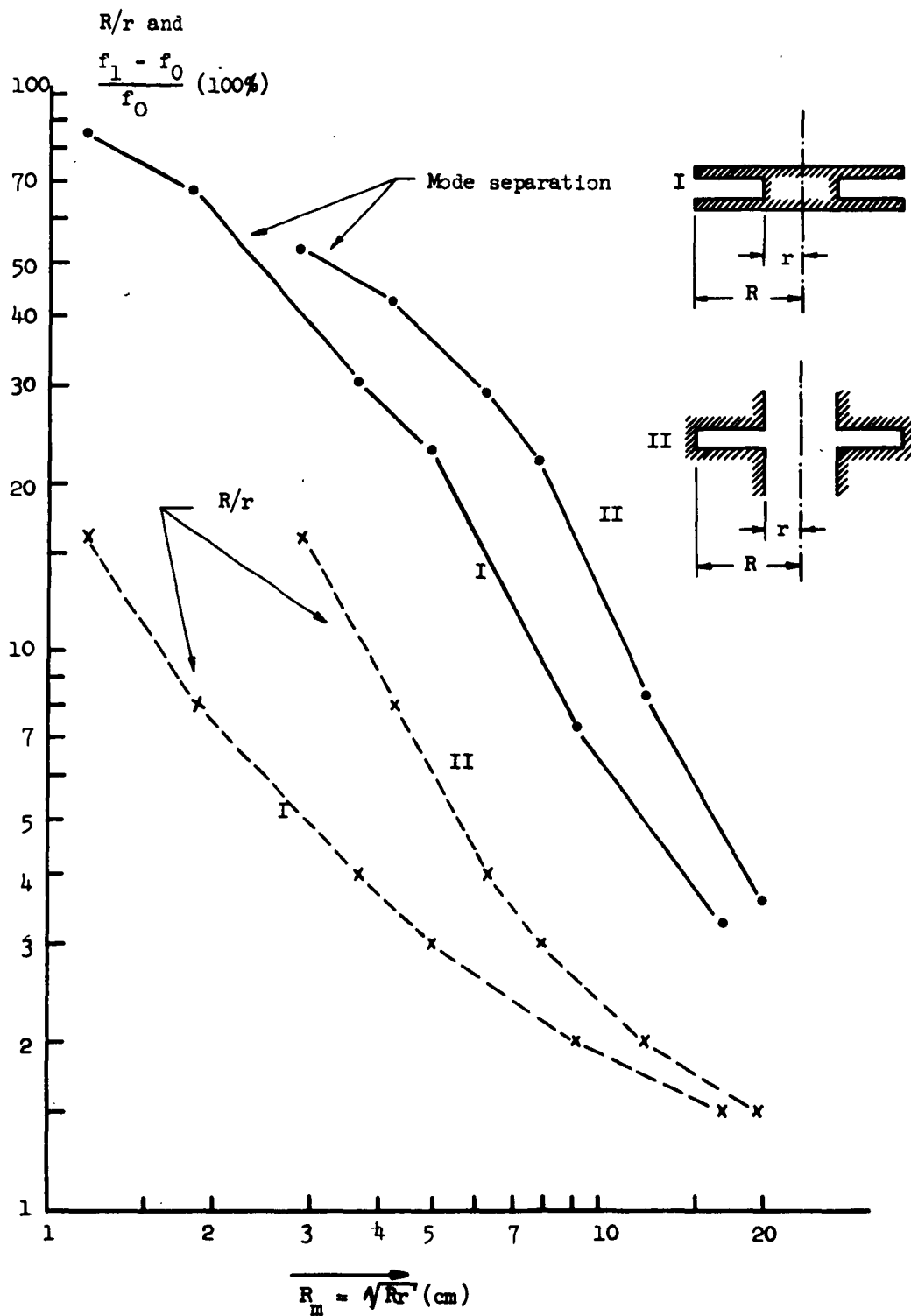


FIG. 29.--Mode separation and  $R/r$  ratio as a function of mean radius  $(Rr)^{1/2}$ .

Table 6.--  $x = 2\pi r/\lambda_0$  for various  $\xi$  and  $\eta$ .

$\eta$	Mode (n)	$\xi = 4$ $\xi_1 = 2$	$\xi = 4$ $\xi_1 = 3$	$\xi = 2$ $\xi_1 = 1.5$
1	0	0.666	0.666	1.80
	1	0.860	0.860	1.95
4	0	0.433	0.418	1.08
	1	0.763	0.673	1.35
8	0	0.325	0.313	0.775
	1	0.755	0.608	1.14
1	$\frac{f_1 - f_0}{f_0}$	29.1%	29.1%	8.33%
4		76.0%	61.0%	25.6%
8		132.0%	94.3%	46.5%

geometric mean radius  $R_m = Rr$ . We see that for a fixed effective size the conventional magnetron has a better mode separation.

#### IV. ANODE-STRUCTURE CONSIDERATIONS

##### A. REDUCTION OF OUTER RADIUS

The structure of Fig. 30 is proposed as a means of reducing the size of the anode.

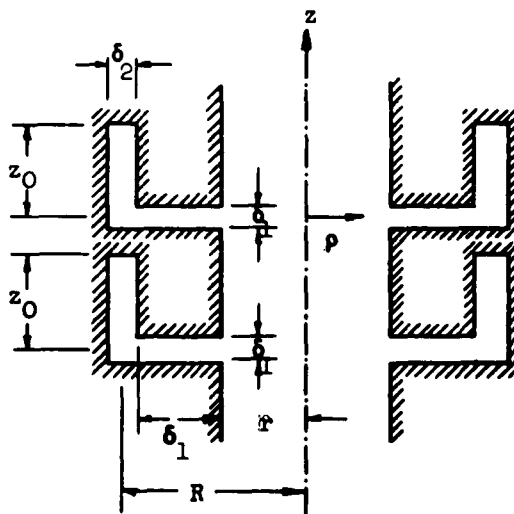


FIG. 30.--Proposed reduced-size anode.



#### (IV. ANODE CONSIDERATIONS)

This structure is analyzed for the  $n = 0$  mode with the assumption of  $R \gg \delta$  and of the boundary conditions of continuous voltage and current at  $z = 0, \rho = R$ . The resonant frequency is determined by

$$\frac{\delta_2}{\delta_1} \tan \beta_0 z_0 = \frac{J_0'(\beta_0 r) N_0(\beta_0 R) - N_0'(\beta_0 r) J_0(\beta_0 R)}{N_0'(\beta_0 r) J_0'(\beta_0 R) - J_0'(\beta_0 r) N_0'(\beta_0 R)} \quad (28)$$

where  $\beta_0 = \omega \sqrt{\mu_0 \epsilon_0}$ . Table 7 gives the results for both the  $n = 0$  and  $n = 1$  modes.

Table 7.-- $2\pi r/\lambda_0$ ( $= \beta r$ ) for $R/r = 2$				
n	$\frac{z_0/r}{\delta_2/\delta_1}$	$\frac{1}{2}$	1	2
0	1	1.20	0.875	0.575
	2	0.965	0.696	0.470
	3	0.835	0.605	0.405
1	1	$\sim 1.4$	$\sim 1.1$	$\sim 0.76$
	2	$\sim 1.2$	$\sim 0.9$	$\sim 0.67$
	3	$\sim 1.06$	$\sim 0.78$	$\sim 0.55$

An experimental structure with  $r = 26$  mm,  $R/r = 2$ ,  $z_0/r = 1$ ,  $\delta_2 = 3$  mm, and  $\delta_1 = 1.5$  mm was used to test the calculated results. The measured frequencies were 1305 Mc ( $n = 0$ ) and 1752 Mc ( $n = 1$ ). The calculated values were 1286 Mc ( $n = 0$ ) and 1645 Mc ( $n = 1$ ).

#### B. MAGNETRON STRUCTURE WITH LARGE MODE SEPARATION

The conventional-magnetron structure shown in Fig. 3la has good mode separation. The structure shown in Fig. 3lb is one half of a simplified version of the structure, suitable for calculation of frequencies.

The lower resonances are given by

$$\tan \frac{\pi \beta x}{2} = \frac{2b}{\delta} \cot x_0 \beta_x \quad (29)$$

and

# (IV. ANODE CONSIDERATIONS)

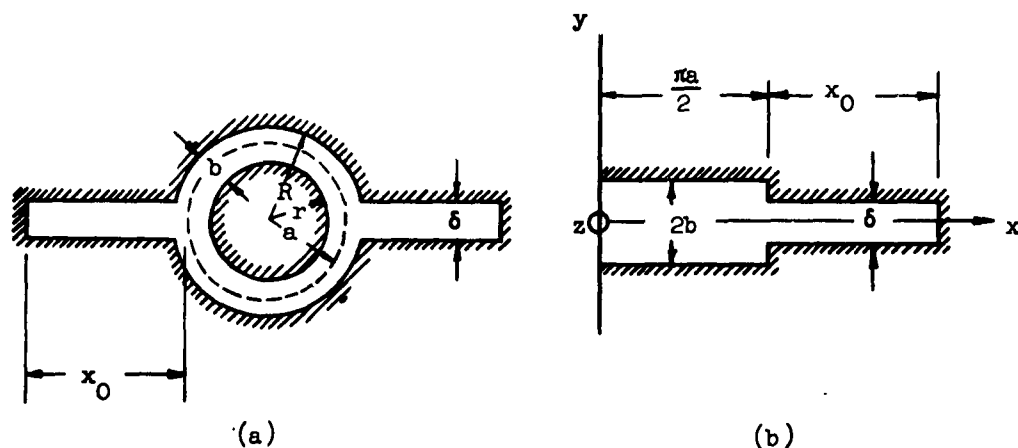


FIG. 31.--Structure with improved mode separation: (a) proposed model (length  $z_0$  along axis); (b) simplified model (open-ended at  $z = \pm z_0/2$ ).

$$\frac{\pi^2}{4z_0^2} + \beta_x^2 = \omega^2 \mu_0 \epsilon_0 = \beta^2$$

The lowest frequency is given by  $\beta_x = \beta$ . The results from these equations are given in Table 8 and as can be seen the mode separation is the better the shorter  $z_0$ . Values of 100 per cent or more are easily obtained. However, this structure is not satisfactory for high-power operation.

Table 8.--Resonant frequencies in terms of $\beta a$ .							
$\frac{x_0}{a}$	$\frac{b}{\delta}$	$\beta = \beta_x$		$\beta^2 = \beta^2 + \pi^2/4z_0^2$		Mode separation	
		First mode	Next mode	$z_0/a = 1$	$z_0/a = 2$	$z_0/a = 1$	$z_0/a = 2$
1	1	0.725	1.75	1.73	1.07	139%	47.6%
	2	0.826	1.70	1.78	1.13	106%	36.8%
2	1	0.528	1.24	1.66	0.946	134%	79.2%
	2	0.611	1.16	1.68	0.994	90.1%	62.6%

#### (IV. ANODE CONSIDERATIONS)

##### C. OUTER-CATHODE ANODE STRUCTURE WITH SHORT-CIRCUITING BARS ALONG OUTER EDGE

Inside the cavity of Fig. 32, the fields are given by the following expressions:

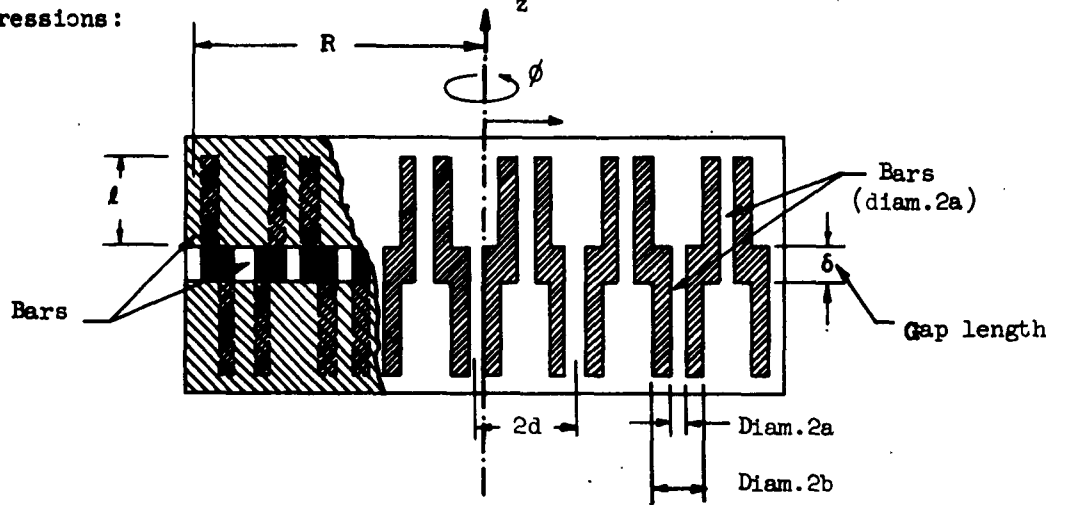


FIG. 32.--Anode structure with outer short-circuiting bars.

$$E_z = E_0 J_0(k\rho) \cos n\phi \quad (30)$$

where  $k = 2\pi/\lambda_n$  and  $\lambda_n$  is the wavelength in free space for the  $n$ th mode. Then

$$H_\rho = -j \frac{nE}{\omega \mu_0} J_n(k\rho) \sin n\phi = -j \frac{nE}{k\rho \mu_0} J_n(k\rho) \sin n\phi$$

$$H_\phi = -j \frac{kE}{\omega \mu_0} J_n'(k\rho) \cos n\phi = -j \frac{\epsilon_0}{\mu_0} E J_n'(k\rho) \cos n\phi$$

The capacitance between two adjacent bars and the inductance for each bar are assumed to be given by

$$\omega C = \frac{\pi \delta}{R} \sqrt{\frac{\epsilon_0}{\mu_0}} \frac{kR}{\log \left( \frac{d + d^2 - 4a^2}{2a} \right)} \quad (31)$$

$$\omega L = \frac{1}{2\pi} \sqrt{\frac{\mu_0}{\epsilon_0}} \log \left( \frac{b}{a} \right) \tan kR \left( \frac{l}{R} \right)$$

Since the boundary condition is taken as

$$-\frac{H_0 d}{\delta E_z} \bigg|_{\rho=R} = j\omega C + \frac{1}{j\omega L} \quad (32)$$

## (IV. ANODE CONSIDERATIONS)

we obtain, from Eqs. (28) through (30),

$$\frac{J'_n(kR)}{J_n(kR)} = -\frac{2\pi\delta}{d} \left[ \log \frac{b}{a} \tan \left( kR \frac{l}{R} \right) \right]^{-1} + \frac{\pi\delta^2}{Rd} \frac{kR}{\log[(d + \sqrt{d^2 - 4a^2})/2a]} \quad (33)$$

Some numerical results derived from Eqs. (31) are shown in Table 9.

Table 9.--Results for Fig. 32.							
$\frac{l}{R}$	$\frac{b}{a}$	$\frac{d}{a}$	$\frac{d}{\delta}$	$\frac{R}{\delta}$	$k_0 R$	$k_1 R$	$\frac{f_1 - f_0}{f_0}$
$\frac{1}{4}$	1.56	2	2.5	12	2.28	3.58	0.57
$\frac{1}{4}$	2	2	4	20	2.14	3.30	0.54
$\frac{1}{10}$	2	2	1	10	2.40	3.83	0.60

## D. CYLINDRICAL CAVITY

Some experiments in this Laboratory have made use of the TE-mode structure depicted schematically in Fig. 33. The resonant frequencies of this structure are given by

$$J'_n(kR) = 0 \quad (34)$$

For the  $n = 0$  mode the frequency separation is 20.3% assuming no variation of the fields along the axis. To realize this situation in practice, end cavities such as shown in Fig. 34 must be used. The dimensions of the end cavity are obtained by solving Maxwell's equations subject to the boundary condition of  $E_\phi = j\sqrt{\mu_0/\epsilon_0} H_0 J'_0(k\rho)$  for  $0 \leq \rho \leq R$ , and  $E_\phi = 0$  for  $R \leq \rho \leq R_1$  at the plane  $z = 0$ . The expression for  $E_\phi$  at  $z = 0$  is

$$E_\phi = \sum_{s=1}^{\infty} A_s J_1(k_s \rho)$$

(IV. ANODE CONSIDERATIONS)

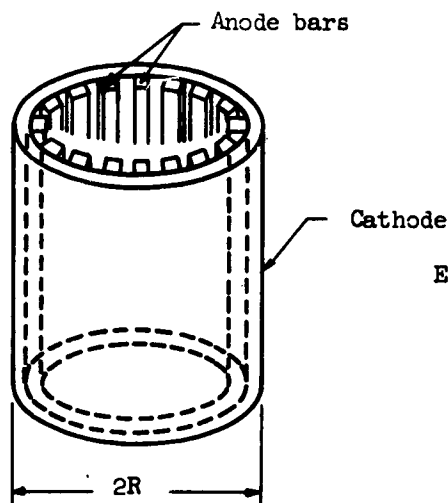


FIG. 33.--TE-mode structure.

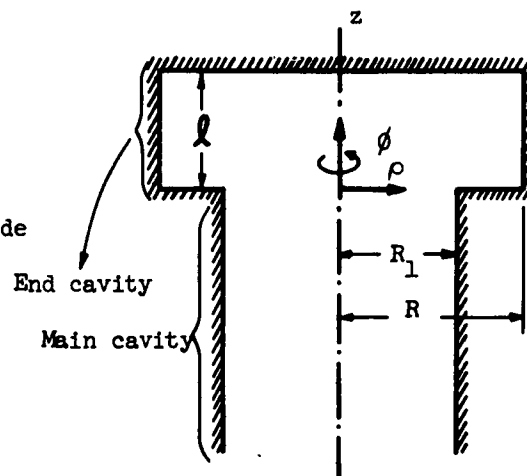


FIG. 34.--End cavities for TE-mode structure.

$$A_s = -j \sqrt{\frac{\mu_0}{\epsilon_0}} \frac{H_0}{R_1^2} \frac{2}{J_2^2(k_s R_1)} \int_0^R J_1(k\rho) J_1(k_s \rho) \rho \, d\rho \quad (35)$$

where  $k_s R_1$  are the roots of  $J_1(x) = 0$ .

Matching only the first term, the approximate cavity dimensions are

$$\left(\frac{l}{R}\right)^2 = \frac{0.168(R_1/R)^2}{(R_1/R)^2 - 1} \quad (36)$$

The matching condition for the s-th mode

$$\left(\frac{l}{R}\right)^2 = \frac{\pi^2 \left(\frac{1}{2} + m\right)^2}{(k_s R_1)^2} \frac{(R_1/R)^2}{(R_1/R)^2 - 1} \quad (37)$$

where  $m$  is an integer.

## V. CONCLUSIONS

Resonant frequencies and mode separation have been determined for a conventional and for an inverted magnetron structure. These structures were chosen for their desirability as high-power magnetron circuits from the point of view of having the largest possible interaction volume.

It is shown that the circuits proposed here have a better mode separation than conventional structures such as the "rising sun."<sup>4</sup>

The structures proposed are easier to fabricate than conventional circuits.

## REFERENCES

1. C. W. Hartman, "Production and interactions of electron beams in crossed fields," Series 60, Issue 325, University of California (Electronics Research Laboratory), 31 October 1960.
2. S. P. Yu and P. N. Hess, "Slow-wave structures for M-type devices," IRE Trans. ED-9: 51-57, 1962.
3. J. R. Pierce, "Traveling-Wave Tubes," Bell Syst. Tech. J. 29:390-460, 1950.
4. G. B. Collins, "Microwave Magnetrons" (vol. 6, M.I.T. Rad. Lab. Series), McGraw-Hill Book Co., New York, 1948; pp. 739-796.

**DISTRIBUTION LIST**  
Contract No. AF 19(628)-324

ORGANIZATION	NO. COPIES	ORGANIZATION	NO. COPIES	ORGANIZATION	NO. COPIES
AFMTC (AFMTC Technical Library-MU-135) Patrick Air Force Base Florida	1	U. S. Army Aviation Human Research Unit U. S. Continental Army Command P. O. Box 428, Fort Rucker, Alabama ATTN: Maj. Arne H. Eliasson	1	General Telephone & Electronics Laboratories, Inc. Bayview Laboratories Bayview 60, New York ATTN: D. Lanza, Mgr., Proj. Adm.	1
AUL Maxwell Air Force Base, Alabama	1	Library Boulder Laboratories National Bureau of Standards Boulder, Colorado	1	Eitel-McCullough, Inc. 798 San Mateo Ave San Francisco, California ATTN: Donald H. Preist	1
OAR (RROS, Col. John R. Fowler) Tempo D 4th and Independence Ave. Washington 25, D. C.	1	Defence Research Member Canadian Joint Staff 2450 Massachusetts Ave., N. W. Washington 8, D. C.	3	Varian Associates 611 Hansen Way Palo Alto, California ATTN: Dr. Richard B. Nelson	2
AFOSR, OAR (SRYP) Tempo D 4th and Independence Ave. Washington 25, D. C.	1	Institute of the Aerospace Sciences, Inc. 2 East 64th St. New York 21, New York ATTN: Librarian	1	Varian Associates 611 Hansen Way Palo Alto, California ATTN: E. W. Herold Vice President, Research	1
ASD (ASNXXR) Wright-Patterson Air Force Base Ohio	1	Massachusetts Institute of Technology Research Laboratory Building 26, Room 327 Cambridge, 39, Massachusetts ATTN: John H. Hewitt	1	Lockheed Aircraft Corporation Missiles & Space Division Technical Information Center 3251 Hanover Street Palo Alto, California ATTN: W. A. Kosumplik, Mgr.	1
RADC (RAALD) Griffiss Air Force Base, New York ATTN: Documents Library	1	Alderman Library University of Virginia Charlottesville, Virginia	1	AVCO Manufacturing Company 2385 Revere Beach Parkway Everett 49, Massachusetts ATTN: Dr. A. R. Kanrowitz	1
Air Force Missile Development Center (MDGRT) Holloman Air Force Base, New Mexico	1	Hq. ARCLL, OAR (CRTPM) L. G. Hanscom Field Bedford, Massachusetts	1	Phillips Laboratories Division of North American Phillips Co., Inc. Irvington on Hudson, New York ATTN: William F. Arnett, Security Officer	1
Hq. OAR (RROSP, Maj. Richard W. Nelson) Washington 25, D. C.	1	Hq. AFCLL, OAR (S. Herskovits) CRDM-1 L. G. Hanscom Field Bedford, Massachusetts	5	Research Technology Associates, Inc. 100 Lodge Drive Electronic Park at Avon Avon, Massachusetts ATTN: J. Babakian	1
Commanding General USASDL Ft. Monmouth, New Jersey ATTN: Technical Documents Center SIGRA/SL-ADT	1	Directorate of Development Planning DCS Research & Technology Hq. USAF (AFRDP-2, Michael Lorenzo) Washington, 25, D. C.	1	Raytheon Company Norwood Plant 415 Providence Highway Norwood, Massachusetts ATTN: L. C. Edwards	1
Department of the Army Office of the Chief Signal Officer Washington 25, D. C. ATTN: SIGRD-4a-2	1	RADC (RALTP, A. Wijek) Griffiss Air Force Base, New York	1	ARO, Inc. AEDC Library Arnold Air Force Station, Tennessee	2
Commanding Officer Diamond Ordnance Fuse Laboratories Washington 25, D. C. ATTN: ORDTL-012	1	RADC (RALSR, Leonard Strauss) Griffiss Air Force Base, New York	1	Rocketdyne 6633 Canoga Avenue Canoga Park, California ATTN: Dr. R. H. Boden, Dept. 584-370	1
Redstone Scientific Information Center U. S. Army Missile Command Redstone Arsenal, Alabama	1	ASD (ASRMPE, Mr. Richard Rivir) Wright-Patterson Air Force Base, Ohio	1	Aero Chem Research Laboratories, Inc. P. O. Box 12 Princeton, New Jersey ATTN: Dr. Calcoe	1
Defense Documentation Center (DDC) Cameron Station Alexandria, Virginia	10	Advisory Group on Electron Devices (AGED) Office of the Director of Defense R&E 346 Broadway, 8th Floor New York 13, New York	4	Litton Systems, Inc. 336 N. Foothill Road Beverly Hills, California ATTN: Space Sciences Laboratory	1
Office of Scientific Intelligence Central Intelligence Agency 2430 E Street, N. W. Washington 25, D. C.	1	Bell Telephone Laboratories, Inc. Whippany Laboratory Whippany, New Jersey ATTN: Technical Information Library	1	Hughes Research Laboratories Malibu, California ATTN: Dr. M. R. Currie	1
Scientific and Technical Information Facility ATTN: NASA Representative (S-AK/DL) P. O. Box 5700 Bethesda, Maryland	1	Technical Library General Electric TWT Products Section 601 California Ave. Palo Alto, California ATTN: Librarian	1	Westinghouse Electric Corp. Box 284 Elmira, New York ATTN: D. C. Buck, Head Microwave Research & Development	1
Director Langley Research Center National Aeronautics and Space Administration Langley Field, Virginia	1	General Electric Advanced Electronics Center Tompkins County Airport Ithaca, New York ATTN: Mr. F. M. Perry	1	Teledyne Systems Corp. 1625 East 126th St. Hawthorne, California ATTN: M. D. Adcock, Director Electromagnetic Systems Division	1
Chief, Bureau of Naval Weapons Department of the Navy Washington 25, D. C. ATTN: DLI-31	1	Eitel-McCullough, Inc. 301 Industrial Way San Carlos, California ATTN: Librarian	1	Linde Company 1500 Polco St. Speedway 24, Indiana ATTN: Dr. M. Stern	1
Director (Code 2027) U. S. Naval Research Laboratory Washington 25, D. C.	1	Sylvania Electric Products, Inc. Electronic Defense Laboratory 123 N. Whisman Road Mountain View, California ATTN: Library	1	S-F-D Laboratories, Inc. 800 Rahway Avenue Union, New Jersey	1
Director, USAF Project RAND The Rand Corporation 1700 Main Street Santa Monica, California THRU: AF Liaison Office	1	Division of Sperry Rand Corporation Sperry Gyroscope Company Great Neck, Long Island, New York ATTN: Eng. Librarian	1	F. J. Liberators, Code 7420 U. S. Naval Research Laboratory Washington 25, D. C.	1
AFCLL, OAR (CRXRA-Stop 39) L. G. Hanscom Field Bedford, Mass.	10	General Electric Company Power Tube Department Electronic Components Division Building 269, Room 205 One River Road Schenectady 5, New York	1		
Aero Research Laboratory (OAR) AROL Library AFL 2292 Building 450 Wright-Patterson Air Force Base, Ohio	1				

<p>Electronics Research Directorate, Air Force Cambridge Research Laboratories, Office of Aerospace Research, U.S. Air Force, Bedford, Mass. Rpt. No. AFRL-63-320, ANODE STRUCTURES FOR COLD-CATHODE HIGH-POWER MAGNETRON Interim Report, June 1962, 43 pp., incl. illus., 4 refs.</p> <p>Unclassified Report</p> <p>Rf interaction properties of several structures suitable for cold-cathode high-power magnetrons have been investigated analytically and experimentally, with special emphasis on increasing the understanding of the interaction and maximizing the area of coherent interaction with the electron beam at a given frequency. The structures analyzed were designed for large mode separation, maximum interaction impedance, and easy coupling to the output circuit.</p>	<ol style="list-style-type: none"><li>1. Electron Tubes</li><li>2. Plasma Physics</li></ol> <ol style="list-style-type: none"><li>1. Ithaca, N.Y.</li></ol>	<p>Electronics Research Directorate, Air Force Cambridge Research Laboratories, Office of Aerospace Research, U.S. Air Force, Bedford, Mass. Rpt. No. AFRL-63-320, ANODE STRUCTURES FOR COLD-CATHODE HIGH-POWER MAGNETRON Interim Report, June 1962, 43 pp., incl. illus., 4 refs.</p> <p>Unclassified Report</p> <p>Rf interaction properties of several structures suitable for cold-cathode high-power magnetrons have been investigated analytically and experimentally, with special emphasis on increasing the understanding of the interaction and maximizing the area of coherent interaction with the electron beam at a given frequency. The structures analyzed were designed for large mode separation, maximum interaction impedance, and easy coupling to the output circuit.</p>	<ol style="list-style-type: none"><li>1. Electron Tubes</li><li>2. Plasma Physics</li></ol> <ol style="list-style-type: none"><li>1. Ithaca, N.Y.</li></ol>
<p>Electronics Research Directorate, Air Force Cambridge Research Laboratories, Office of Aerospace Research, U.S. Air Force, Bedford, Mass. Rpt. No. AFRL-63-320, ANODE STRUCTURES FOR COLD-CATHODE HIGH-POWER MAGNETRON Interim Report, June 1962, 43 pp., incl. illus., 4 refs.</p> <p>Unclassified Report</p> <p>Rf interaction properties of several structures suitable for cold-cathode high-power magnetrons have been investigated analytically and experimentally, with special emphasis on increasing the understanding of the interaction and maximizing the area of coherent interaction with the electron beam at a given frequency. The structures analyzed were designed for large mode separation, maximum interaction impedance, and easy coupling to the output circuit.</p>	<ol style="list-style-type: none"><li>1. Electron Tubes</li><li>2. Plasma Physics</li></ol> <ol style="list-style-type: none"><li>1. Ithaca, N.Y.</li></ol>	<p>Electronics Research Directorate, Air Force Cambridge Research Laboratories, Office of Aerospace Research, U.S. Air Force, Bedford, Mass. Rpt. No. AFRL-63-320, ANODE STRUCTURES FOR COLD-CATHODE HIGH-POWER MAGNETRON Interim Report, June 1962, 43 pp., incl. illus., 4 refs.</p> <p>Unclassified Report</p> <p>Rf interaction properties of several structures suitable for cold-cathode high-power magnetrons have been investigated analytically and experimentally, with special emphasis on increasing the understanding of the interaction and maximizing the area of coherent interaction with the electron beam at a given frequency. The structures analyzed were designed for large mode separation, maximum interaction impedance, and easy coupling to the output circuit.</p>	<ol style="list-style-type: none"><li>1. Electron Tubes</li><li>2. Plasma Physics</li></ol> <ol style="list-style-type: none"><li>1. Ithaca, N.Y.</li></ol>



Electronics Research Directorate, Air Force Cambridge Research Laboratories, Office of Aerospace Research, U.S. Air Force, Bedford, Mass.  
Rpt. No. AFRL-63-320. ANODE STRUCTURES FOR COLD-CATHODE HIGH-POWER MAGNETRON.  
Interim Report, June 1962. 43 pp., incl. illus., 4 refs.

Unclassified Report

RF interaction properties of several structures suitable for cold-cathode high-power magnetrons have been investigated analytically and experimentally, with special emphasis on increasing the understanding of the interaction and maximizing the area of coherent interaction with the electron beam at a given frequency. The structures analyzed were designed for large mode separation, maximum interaction impedance, and easy coupling to the output circuit.



1. Electron Tubes
2. Plasma Physics
1. Iteda, Y.

Electronics Research Directorate, Air Force Cambridge Research Laboratories, Office of Aerospace Research, U.S. Air Force, Bedford, Mass.  
Rpt. No. AFRL-63-320. ANODE STRUCTURES FOR COLD-CATHODE HIGH-POWER MAGNETRON.  
Interim Report, June 1962. 43 pp., incl. illus., 4 refs.

Unclassified Report

RF interaction properties of several structures suitable for cold-cathode high-power magnetrons have been investigated analytically and experimentally, with special emphasis on increasing the understanding of the interaction and maximizing the area of coherent interaction with the electron beam at a given frequency. The structures analyzed were designed for large mode separation, maximum interaction impedance, and easy coupling to the output circuit.



Electronics Research Directorate, Air Force Cambridge Research Laboratories, Office of Aerospace Research, U.S. Air Force, Bedford, Mass.  
Rpt. No. AFRL-63-320. ANODE STRUCTURES FOR COLD-CATHODE HIGH-POWER MAGNETRON.  
Interim Report, June 1962. 43 pp., incl. illus., 4 refs.

Unclassified Report

RF interaction properties of several structures suitable for cold-cathode high-power magnetrons have been investigated analytically and experimentally, with special emphasis on increasing the understanding of the interaction and maximizing the area of coherent interaction with the electron beam at a given frequency. The structures analyzed were designed for large mode separation, maximum interaction impedance, and easy coupling to the output circuit.



1. Electron Tubes
2. Plasma Physics
1. Iteda, Y.

Electronics Research Directorate, Air Force Cambridge Research Laboratories, Office of Aerospace Research, U.S. Air Force, Bedford, Mass.  
Rpt. No. AFRL-63-320. ANODE STRUCTURES FOR COLD-CATHODE HIGH-POWER MAGNETRON.  
Interim Report, June 1962. 43 pp., incl. illus., 4 refs.

Unclassified Report

RF interaction properties of several structures suitable for cold-cathode high-power magnetrons have been investigated analytically and experimentally, with special emphasis on increasing the understanding of the interaction and maximizing the area of coherent interaction with the electron beam at a given frequency. The structures analyzed were designed for large mode separation, maximum interaction impedance, and easy coupling to the output circuit.



1. Electron Tubes
2. Plasma Physics
1. Iteda, Y.

LIST OF SCIENTIFIC REPORTS PUBLISHED UNDER  
CONTRACT AF 19(628)-324

SR-No. 1: D. H. Sloan, C. Süsskind, and Staff, "Production and control of electron beams," Series No. 60, Issue No. 203, 15 June 1958.

SR-No. 2: V. Bevc, "Injection of space-charge-balanced electron beams for microwave tubes," Series No. 60, Issue No. 204, 15 June 1958.

SR-No. 3: A. J. Lichtenberg, D. H. Sloan, C. Süsskind, J. R. Woodyard, and Staff, "Electron and plasma beam dynamics," Series No. 60, Issue No. 238, 15 June 1959.

SR-No. 4: E. D. Hoag, "Glow cathodes in pulsed magnetic fields," Series No. 60, Issue No. 239, 15 June 1959.

SR-No. 5: J. N. Dukes, "A gaseous-conduction linear amplifier with magnetic focusing," Series No. 60, Issue No. 240, 30 June 1959.

SR-No. 6: B. N. Edwards, "A study of the Hall effect in gaseous conductors," Series No. 60, Issue No. 253, 30 September 1959.

SR-No. 7: J. W. Hansen, "Scheme for improving beam-tube performance by depressing collector potential," Series No. 60, Issue No. 260, 15 December 1959.

SR-No. 8: D. H. Sloan, C. Süsskind, A. W. Trivelpiece, J. R. Woodyard, and Staff, "Electron and plasma beams," Series No. 60, Issue No. 284, 15 June 1960.

SR-No. 9: R. E. Lundgren, "Extraction and modulation of electron beam from Philips ion gage," Series No. 60, Issue No. 306, 31 August 1960.

SR-No. 10: C. W. Hartman, "Production and interactions of electron beams in crossed fields," Series No. 60, Issue No. 325, 31 October 1960.

SR-No. 11: D. R. Noel, "Special deflection systems for cathode-ray tubes," Series No. 60, Issue No. 329, 2 December 1960.

SR-No. 12: B. E. Dobratz, "A study of circuit-independent oscillations in a gaseous conductor," Series No. 60, Issue No. 344, 15 February 1961.

SR-No. 13: J. F. Fry, "The effects of rf energy on the pumping speed of a titanium sputter pump," Series No. 60, Issue No. 355, 18 April 1961.

SR-No. 14: B. Maxum and A. W. Trivelpiece, "Cyclotron-wave nonconvective instability," Series No. 60, Issue No. 379, 1 July 1961.

SR-No. 15: G. August, "Coulomb collisions in strong rf electric fields," Series No. 60, Issue No. 397, 24 August 1961.

SR-No. 16: G. August, "Plasma confinement of electromagnetic waves," Series No. 60, Issue No. 398, 24 August 1961.

SR-No. 17: Y. Ikeda, "Behavior of the space charge in a plasma magnetron," Series No. 60, Issue No. 433, 15 June 1962.

SR-No. 18: M. Chamran, "Electron beam in the cold-cathode magnetron," Series No. 60, Issue No. 453, 15 June 1962.

SR-No. 19: B. E. Dobratz, "Positive-column striations in gaseous conductors," Series No. 60, Issue No. 454, 19 June 1962.

SR-No. 20: Y. Ikeda, "Anode structures for cold-cathode high-power magnetron," Series No. 60, Issue No. 455, 30 June 1962.

SR-No. 21: L. Spinazze, "Dc electroluminescence in manganese-activated aluminum-oxide films," Series No. 60, Issue No. 482, 11 September 1962.